J. Fluid Mech. (2014), *vol.* 751, *pp.* 539–569.
doi:10.1017/jfm.2014.303

Critical layer and radiative instabilities in shallow-water shear flows

Xavier Riedinger† and Andrew D. Gilbert

College of Engineering, Mathematics and Physical Sciences, University of Exeter, Exeter EX4 4QF, UK

(Received 5 August 2013; revised 14 March 2014; accepted 27 August 2014; first published online 23 June 2014)

In this study a linear stability analysis of shallow-water flows is undertaken for a representative Froude number $F = 3.5$. The focus is on monotonic base flow profiles U without an inflection point, in order to study critical layer instability (CLI) and its interaction with radiative instability (RI). First the dispersion relation is presented for the piecewise linear profile studied numerically by Satomura (*J. Meterol. Soc. Japan*, vol. 59, 1981, pp. 148–167) and using WKBJ analysis an interpretation given of mode branches, resonances and radiative instability. In particular surface gravity (SG) waves can resonate with a limit mode (LM) (or Rayleigh wave), localised near the discontinuity in shear in the flow; in this piecewise profile there is no critical layer. The piecewise linear profile is then continuously modified in a family of nonlinear profiles, to show the effect of the vorticity gradient $Q' = -U''$ on the nature of the modes. Some modes remain as modes and others turn into quasi-modes (QM), linked to Landau damping of disturbances to the flow, depending on the sign of the vorticity gradient at the critical point. Thus an interpretation of critical layer instability for continuous profiles is given, as the remnant of the resonance with the LM. Numerical results and WKBJ analysis of critical layer instability and radiative instability for more general smooth profiles are provided. A link is made between growth rate formulae obtained by considering wave momentum and those found via the WKBJ approximation. Finally the competition between the stabilising effect of vorticity gradients in a critical layer and the destabilising effect of radiation (radiative instability) is studied.

Key words: critical layers, free shear layers, shallow water flows

1. Introduction

Fluid mechanical phenomena in astrophysics and geosciences are a motivation for the study of shear instability in shallow, stratified, rotating fluid layers. Many types of waves and instabilities can occur, and the investigation of very idealised models is relevant to teasing out mechanisms and interactions, especially in linear regimes. In this paper we consider fluid flow governed by the shallow-water (or Saint Venant) equations in a Cartesian geometry (without imposed rotation). Here a natural class of problems involves understanding the instabilities of a shear flow of constant depth bounded on one side by an impermeable boundary (here $y = 0$)

† Email address for correspondence: xavier.riedinger@gmail.com

and unbounded on the other side. A range of profiles $U(y)$ can be considered as models of possible flows adjacent to the boundary, for example modelling a boundary current in an ocean. A piecewise linear profile was studied numerically by Satomura (1981). In this case with an open domain, he obtained a family of surface gravity modes (SGM) (localised near the boundary) and a single branch of modes linked to the discontinuity in the slope U' of the profile. He observed resonances between these modes and the presence of radiative instability (RI), in which an unstable mode incorporates waves that propagate to infinity, with outwards group velocity. For any piecewise linear shallow-water flow an exact dispersion relation may be written in terms of Kummer functions, and this is done for the Satomura (1981) profile by Knessl & Keller (1995); those authors did not develop this further, and we note that these dispersion relations are sufficiently unwieldy that asymptotic approximations are needed to extract useful information. Glatzel (1985) discusses a related stability equation for a compressible shear flow, with Kelvin–Helmholtz instability resulting from resonances between modes localised at the two discontinuities of the profile.

When the profile $U(y)$ is no longer piecewise linear the possibilities for instabilities become richer, while exact solutions can no longer be written down. A key study is Balmforth (1999) for linear and nonlinear shear flow profiles confined to a channel; that author identifies three kinds of instabilities. First there is the classical inflectional instability (Rayleigh 1880; Fjørtoft 1950), present in the Froude number limit $F \to 0$ of incompressible fluid flow, when the surface gravity (SG) wave speed is infinite. Secondly, for $F > 0$ the wave speed becomes finite and waves may be destabilised if there is a critical layer where the wave speed and the flow speed are the same. In this case the behaviour of a mode is closely linked to the potential vorticity gradient in the layer: if its sign is the same as that of the wave momentum M the mode will be destabilised, otherwise it will be damped. The latter process is an example of Landau damping, first explained in the fluid context by Briggs, Daugherty & Levy (1970), as discussed further below. Finally, there is an unstable resonance between pairs of SGM, localised on opposite sides of the channel. For the flows considered in the present paper, this third instability is not present as the flow is bounded only on one side, but a fourth type of instability is allowed, a RI with waves propagating to infinity, away from the wall. Finally for the discontinuous profiles there is the resonance instability obtained by Satomura.

RI was first found in compressible shear flows, in vortices by Broadbent & Moore (1979) and in many works by Lindzen (e.g. Lindzen & Tung 1978; Lindzen & Barker 1985), who first showed that the instability is based on over-reflection. Here waves are trapped and totally internally reflected, and at each reflection a wavepacket draws energy from the underlying shear flow, while at the same time radiating a wavepacket to infinity. Thereafter radiative modes were found in various open flows where both shear and stratification are present, for example in rotating flows, boundary and shear layers, and jets, in the presence of linear stratification, shallow-water dynamics, and compressibility. RI is observed experimentally by Riedinger, Le Dizès & Meunier (2011) in the case of the potential flow around a rotating cylinder in a stratified fluid. For a Froude number and a Reynolds number at the marginal stability limit, two networks of internal waves are generated, one corresponding to a helicoidal wave going down the cylinder and the other going up. There are several ways of viewing the instability mechanism: it may be seen as an over-reflection process (Takehiro & Hayashi 1992), as a consequence of the conservation of wave activity or pseudomomentum (Schecter & Montgomery 2004), or in terms of a reversal of the wave group velocity (Le Dizès & Billant 2009).

A WKBJ analysis may be employed in these linear problems to obtain growth rates and to understand the over-reflection process and the role of the critical layer and turning points. Stratified vortices are considered in papers by Le Dizès and co-workers, for example Le Dizès & Billant (2009). For these flows the dominant term in the growth rate arises from radiation and a secondary damping term results from the critical layer. The competition between radiation and critical layer damping has also been studied in Schecter & Montgomery (2004) and Park & Billant (2012, 2013). In a recent work on compressible jets (Parras & Le Dizès 2010), a WKBJ analysis for radiative modes shows that the term in the growth rate resulting from the over-reflection at the critical level can also be destabilising.

Critical layers are better known for their stabilising effect, as for example explained in Briggs *et al.* (1970). Modes are found to be damped by a fluid–wave interaction similar to the Landau damping of plasma oscillations. In the fluid context this amounts to the generation of vorticity fluctuations in the presence of a background vorticity gradient, and the feedback on the mode as they are sheared out in the local flow. The mechanism is intimately linked to conservation of potential vorticity. Mathematically the resulting linear perturbation is not described by a normal mode and to obtain the decay rate the linear eigenvalue problem has to be integrated on a complex contour which cannot be deformed to the real axis. The corresponding eigenvalue is called a Landau pole, and is associated with a quasi-mode (QM), which can be considered as formed from the continuous spectrum, in other words a combination of singular modes that naturally arises in the initial value problem (Briggs *et al.* 1970). QMs always have a damping effect on perturbations, an effect studied for vortices, and nonlinear effects can lead to the formation of structures such cat's eyes or tripoles (e.g. Rossi, Lingevitch & Bernoff 1997; Balmforth 1999; Bassom & Gilbert 1999; Schecter *et al.* 2000; Balmforth, Llewellyn Smith & Young 2001; Turner, Gilbert & Bassom 2008), also observed in experiments (van Heijst 1991). Growth of unstable modes whose structure includes a critical layer has been observed in experiments on a columnar vortex in a stratified fluid (Riedinger, Meunier & Le Dizès 2010*b*). Little work has been published on the potential destablising effect of a critical layer, in particular for model geophysical flows, although it has been identified as the effect of a gradient in the background potential vorticity by Kubokawa (1985), Papaloizou & Pringle (1987) and Perkins & Renardy (1997). Otherwise the term 'critical layer instability (CLI)', although it is not well established, has been used for baroclinic flows (Bretherton 1966) and two-layer flows (Iga 1999).

The goal of the present paper is to study instabilities of shallow-water shear flows, numerically and analytically, with particular interest in resonances, CLI and RI. The paper is organised as follows. In § 2 the governing equations are given, together with the general WKBJ formulation. The latter leads to a classification of types of modes, depending on the presence of critical points and turning points. Section 3 concerns the piecewise linear profile of Satomura (1981) (see also Knessl & Keller 1995) which is the basis of all our subsequent analysis. We discuss the various modes and resonances, supported by WKBJ and related analysis. In particular we link a branch of 'limit' modes to the discontinuity in the piecewise profile, and give asymptotic formulae for these modes. In § 4 we consider a family of flows which includes the piecewise linear profile of Satomura (1981) but allows a quadratic profile, with non-vanishing vorticity gradient. This highlights the role of the critical layer and, as the profile is distorted from linear, numerical results indicate the effect on the branches and resonances. Importantly critical layer damping or destabilisation can now take place. Some previously neutral branches of modes remain as modes, while others turn into QMs. To give an analytical basis to our results, the piecewise defined profiles are inconvenient, and in § 5 we discuss several smooth profiles. Some are bounded as $y \to \infty$ and some unbounded: in the latter case all modes become radiative at infinity. These profiles have neutral modes that may be stabilised or destabilised by potential vorticity gradients in the critical layer, and may be subject to RI. Asymptotic formulae for these effects are derived using WKBJ theory and matching to local solutions near critical points, and confirmed by means of numerical calculations. Finally § 6 offers concluding discussion.

2. Governing equations

Our study concerns fluid motion governed by the shallow-water equations, which we write in a standard dimensionless form,

$$\partial_t \boldsymbol{u} + \boldsymbol{u} \cdot \nabla \boldsymbol{u} + F^{-2} \nabla h = 0, \tag{2.1}$$

$$\partial_t h + \nabla \cdot (h\boldsymbol{u}) = 0, \tag{2.2}$$

where F is the Froude number based on the SG wave velocity (with $F^2 = U^2/gH$ in dimensional quantities) (e.g. Balmforth 1999), $\boldsymbol{u}$ and h are the disturbances of velocity and depth. The shallow-water dynamics gives material conservation of potential vorticity q,

$$\partial_t q + \boldsymbol{u} \cdot \nabla q = 0, \quad q = h^{-1} \hat{\boldsymbol{z}} \cdot \nabla \times \boldsymbol{u}. \tag{2.3}$$

We consider an unperturbed, or basic, state of a steady shear flow with uniform depth,

$$\boldsymbol{u} = \boldsymbol{U} \equiv U(y)\hat{\boldsymbol{x}}, \quad h = H \equiv 1, \quad q = Q \equiv -U', \tag{2.4a–c}$$

in a half-plane given by $y \geqslant 0$ with an impermeable boundary $y = 0$. The velocity profiles we consider have $U(0) = 1$ and do not have inflection points, which rules out the inflectional instabilities discussed in Balmforth (1999) and Mak, Griffiths & Hughes (2014). Such instabilities are linked to the classical Rayleigh theory, since in the limit $F \to 0$ the shallow-water equations reduce to those for incompressible two-dimensional fluid flow. We consider flows with different limits as $y \to \infty$, with $U \to 0$ for the flows in § § 2–5.2 and unbounded $U(y)$ in § 5.3.

We take the equations for small-amplitude perturbations, make the substitutions

$$\boldsymbol{u} \to (U, 0) + (u(y), v(y))\mathrm{e}^{\mathrm{i}k(x-ct)}, \quad h \to H + h(y)\mathrm{e}^{\mathrm{i}k(x-ct)}, \quad q \to Q + q(y)\mathrm{e}^{\mathrm{i}k(x-ct)}, \tag{2.5a–c}$$

in (2.1), (2.2), and linearise to obtain

$$\mathrm{i}k(U - c)u + U'v + F^{-2}\mathrm{i}kh = 0, \tag{2.6}$$

$$\mathrm{i}k(U - c)v + F^{-2}\partial_y h = 0, \tag{2.7}$$

$$\mathrm{i}k(U - c)h + \mathrm{i}ku + \partial_y v = 0 \tag{2.8}$$

(Balmforth 1999). These govern normal modes of the perturbation fields u, v and h with wavenumber $k \geqslant 0$ in the x direction and (possibly complex) wave speed $c = c_r + \mathrm{i}c_i$. We use a prime to denote a y-derivative of the basic state (only). The perturbation potential vorticity q is given by

$$q = \mathrm{i}kv - \partial_y u - Qh \tag{2.9}$$

and satisfies

$$\mathrm{i}k(U-c)q+Q'v=0. \tag{2.10}$$

The term $Q'v$ gives the generation of perturbation potential vorticity in a background gradient $Q'=-U''$. For a purely linear shear flow, $Q'=-U''=0$, and this generation term is absent, making q identically zero.

A useful quantity is the wave momentum which in the full time-dependent problem is defined by $M\exp(2kc_i t)$, with

$$M=\frac{1}{2}\int_0^\infty (uh^*+hu^*)\,\mathrm{d}y. \tag{2.11}$$

This is given in Balmforth (1999), together with the wave energy E which we do not need here. M is quadratic in the disturbance fields and its time evolution under (2.6)–(2.8) is linked to the transport of perturbation potential vorticity through

$$2kc_iM=-\frac{1}{2}\int_0^\infty (vq^*+qv^*)\,\mathrm{d}y, \tag{2.12}$$

for modes that are evanescent as $y\rightarrow\infty$. For a purely linear profile, $U''=0$, q is zero and so M is conserved; in this case a growing or decaying mode, $c_i\neq 0$, must have zero total momentum M. This is relevant to unstable resonances in bounded shear flows (Hayashi & Young 1987; Takehiro & Hayashi 1992).

2.1. *WKBJ formulation*

The key to understanding numerical results, as well as giving approximations to growth rates and frequencies, is a WKBJ analysis in the limit of large wavenumber $k\gg 1$. Equations (2.6)–(2.8) are a second-order system of ODEs, which may be written in various forms. We first eliminate in favour of h to give

$$\partial_y^2 h-2U'(U-c)^{-1}\partial_y h-k^2\Delta_0 h=0. \tag{2.13}$$

Here Δ_0 is a function of y defined by

$$\Delta_0(y)=1-F^2(U-c)^2. \tag{2.14}$$

Although our numerical work is based on (2.13), for analysis in the limit of large k we eliminate the term in $\partial_y h$ by setting

$$g(y)=(U-c)^{-1}h, \tag{2.15}$$

to give

$$\partial_y^2 g=k^2\Delta\, g, \tag{2.16}$$

where the function $\Delta(y)$ is

$$\Delta(y)=1-F^2(U-c)^2-k^{-2}U''(U-c)^{-1}+2k^{-2}U'^2(U-c)^{-2}. \tag{2.17}$$

WKBJ approximations to (2.16) then involve $\Delta(y)$ in (2.17) in the standard form,

$$g(y)=|\Delta(y)|^{-1/4}\exp\left(\pm k\int^y\sqrt{\Delta(s)}\,\mathrm{d}s\right). \tag{2.18}$$

With reference to (2.14) we may write the quantity $\varDelta(y)$ as

$$\varDelta = \varDelta_0 + k^{-2}\varDelta_1, \quad \varDelta_1 = -U''(U-c)^{-1} + 2U'^2(U-c)^{-2}. \tag{2.19}$$

For large k, the first term $\varDelta_0(y)$ in (2.19) is nominally the largest. This gives rise to oscillatory solutions in regions where $\varDelta_0$ is negative and evanescent behaviour where $\varDelta_0$ is positive. Two adjacent regions are separated by a turning point y_t with

$$\varDelta_0(y_t) = 0, \tag{2.20}$$

and when a mode has two we label them as y_{t1} and y_{t2} with $y_{t1} < y_{t2}$. The other significant feature of (2.19) is the possible presence of a critical point y_c, where the wave speed is equal to the flow velocity and the term involving $\varDelta_1$ can increase, given by

$$U(y_c) = c. \tag{2.21}$$

Except close to a critical point y_c, the terms in $\varDelta_1$ in (2.19) may be neglected compared with $\varDelta_0$. However within a distance of order k^{-1} of the critical point, $\varDelta_1$ increases to become comparable with $\varDelta_0$ and a new expansion must be sought.

For some solution branches, modes are purely oscillatory with real wave speed c, in which case any relevant turning points y_t and critical point y_c will lie on the real y-axis. In other situations, where there is instability or damping, c becomes complex and these points lie in the complex plane. However despite this, our asymptotic calculations are based on $c = c_r + \mathrm{i}c_i$ being approximately real ($c_r = O(1)$, $c_i \ll 1$). For this reason it is helpful to work on the basis that c is real together with real points y_t and y_c, all correct at leading order, and then calculate the small correction c_i perturbatively. In what follows we often speak as if y_t and y_c are real, even though these points may be 'pushed' above or below the real axis by small values of c_i. This approximation is valid, as the magnitude of c_i is found to be exponentially small in terms of k when WKBJ solutions are linked across an evanescent region of finite width (independent of k).

Given a profile $U(y)$, the problem then is to solve (2.13) or (2.16) subject to the boundary condition at the origin of no normal flow, $v = 0$, amounting to

$$h'(0) = 0 \quad \text{or} \quad g'(0)/g(0) = -U'(0)(U(0)-c)^{-1}, \tag{2.22a,b}$$

and to the condition as $y \to \infty$ that

$$h(y) \to 0 \quad \text{or} \quad g(y) \to 0 \quad (y \to \infty), \tag{2.23a,b}$$

for evanescent modes, decaying at infinity. For radiative modes, which are oscillatory as $y \to \infty$, we need instead the radiation condition that waves propagate outwards,

$$h(y)(U-c)^{-1} = g(y) \sim |\varDelta(y)|^{-1/4} \exp\left(\pm\mathrm{i}k\int^y \sqrt{-\varDelta(s)}\,\mathrm{d}s\right), \tag{2.24}$$

with the upper/lower sign for positive/negative c_r. For each applicable set of boundary conditions there results an eigenvalue problem giving branches of modes $c(k)$ for a given value of the Froude number F.

As well as discrete normal modes, there are two branches of continuous spectrum, namely,

$$S_{crit} = \{c : c = U(y), y \in \mathbb{R}\}, \tag{2.25}$$

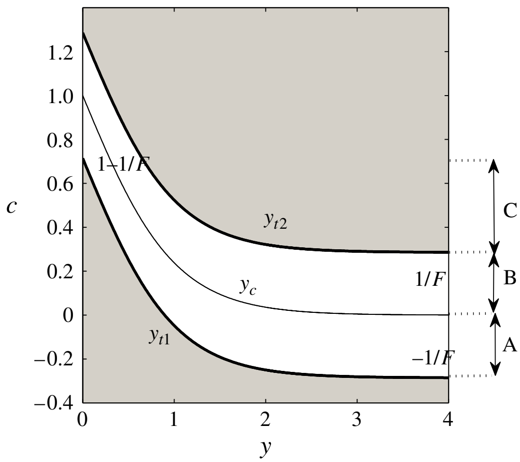

FIGURE 1. Location of turning and critical points, and sign of Δ_0, in the (y, c_r)–plane with $c = c_r$ real, according to the profile $U_2 = 1 - \tanh y$ with $F = 3.5$. The shaded zones correspond to $\Delta_0 < 0$ and oscillatory modes. The turning points y_{t1}, y_{t2} are marked by thick curves and the critical point y_c by a thinner curve.

$$S_{rad} = \{c : \Delta_0(\infty) < 0\} = \{c : c > U(\infty) + F^{-1} \text{ or } c < U(\infty) - F^{-1}\}. \tag{2.26}$$

The first branch is linked to the presence of critical points y_c on the real axis where the differential equation is singular and the second is a range of values of c for which there are outward-going waves at great distances (cf. Riedinger, Le Dizès & Meunier 2010*a*). These branches correspond to an integration contour $y \in \mathbb{R}$ for (2.13) or (2.16), but they can be deformed in the complex plane by distorting this contour.

2.2. *Classes of modes*

For a given profile $U(y)$ there are several distinct classes of WKBJ solutions depending on the presence and location of turning and critical points. To illustrate this and establish notation, we take the smooth profile $U(y) = 1 - \tanh y$ (shown as U_2 in figure 2(*b*) below) with $F = 3.5$ as an example, and consider real values of $c = c_r$, plotted on the vertical axis in figure 1. For each value of c we show the location of the turning points y_{t1}, y_{t2} given by (2.20) (solid curves) on the horizontal axis, together with the critical point y_c from (2.21) (thin curve). In the shaded regions $\Delta_0 < 0$ and the WKBJ solution is oscillatory; otherwise the solution is exponential.

Given a value of c we may read horizontally to find turning and critical points, and so identify the following classes of modes:

(*a*) class A, $c_r \in (-F^{-1}, 0)$: modes that are oscillatory for $[0, y_{t1}]$, evanescent for larger values of y and with no critical point;

(*b*) class B, $c_r \in (0, F^{-1})$: as for class A but with a critical point y_c in the open evanescent region;

(*c*) class C, $c_r \in (F^{-1}, 1 - F^{-1})$: modes that are oscillatory in $[0, y_{t1}]$ and for $y > y_{t2}$ with an evanescent region in between; these are radiative modes.

From the figure, radiative modes in class C exist when $F^{-1} < 1 - F^{-1}$, that is $F > 2$, and modes in class B exist when $1 - F^{-1} > 0$, that is $F > 1$. For the present study we fix a representative value of the Froude number $F = 3.5$ for all our simulations,

https://doi.org/10.1017/jfm.2014.303 Published online by Cambridge University Press

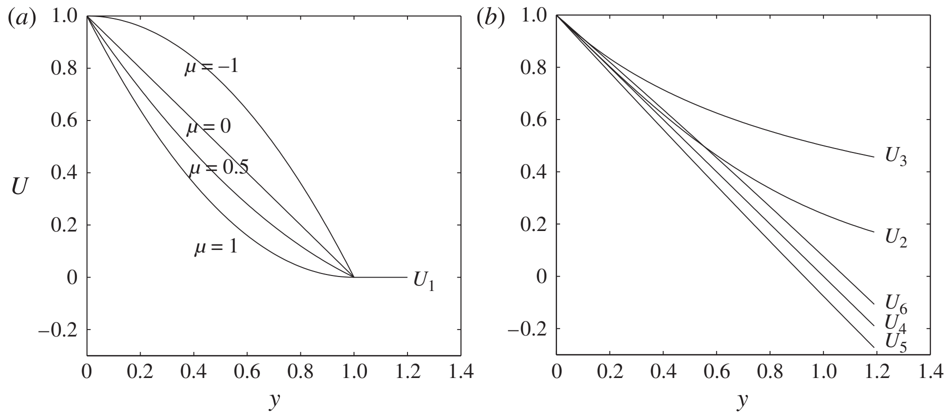

FIGURE 2. Basic flow profiles. (*a*) Flow profiles U_1 that are zero for $y \geqslant 1$ and given by (4.1). The case $\mu = 0$ gives the piecewise linear profile U in (3.1). (*b*) Everywhere smooth profiles U_2 and U_3 in (5.1), U_4 in (5.19), U_5 in (5.20), and U_6 in (5.21).

as this gives all three classes of modes. The sketch of modes in figure 1 is similar to the one obtained by Parras & Le Dizès (2010) for a study of instability in a compressible round jet: class A modes correspond to counterflow waves, class B to subsonic coflow waves, and class C to supersonic coflow waves. Note that in figure 1 the characteristics of the modes are plotted according to the real part of the velocity c_r, but also constitute the leading-order approximation when $c_i \ll 1$ and modes are weakly damped or destabilised

3. Piecewise linear profile

The starting point for our study is the piecewise linear profile of Satomura (1981),

$$U(y) = \begin{cases} 1 - y & (0 \leqslant y \leqslant 1), \\ 0 & (y > 1). \end{cases} \tag{3.1}$$

This is the profile with $\mu = 0$ shown in figure 2(*a*). The piecewise linear property means that there is zero potential vorticity gradient $Q' = -U''$, except for a delta-function concentration at $y = y_d = 1$. This allowed Knessl & Keller (1995) to write down an exact but awkward dispersion relation in terms of Kummer functions. We will not proceed in this way, but instead apply WKBJ approximations from the outset below; this allows easier generalisation to profiles that are not piecewise linear in later sections.

As $U = 0$ for $y > 1$ we may write g in (2.16) as a decaying exponential satisfying (2.23),

$$g \propto \exp\left(-ky\sqrt{1 - F^2c^2}\right), \tag{3.2}$$

or a wave with the appropriate sign for the radiation condition given in (2.24),

$$g \propto \exp\left(\pm iky\sqrt{F^2c^2 - 1}\right). \tag{3.3}$$

The solution is required to have h and h' continuous across $y = 1$; the latter makes the normal flow component v continuous there but there is generally a discontinuity

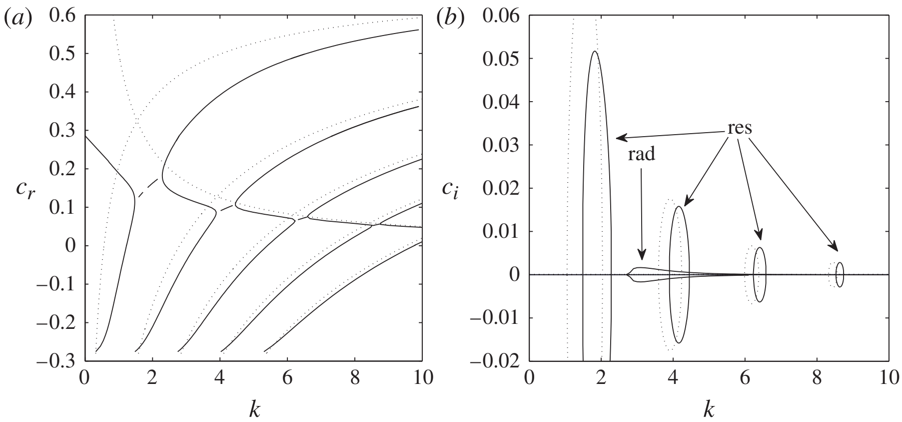

FIGURE 3. (*a*) Frequency c_r and (*b*) growth rate c_i for $F = 3.5$ and the piecewise linear profile (3.1). In each case the solid lines give the numerical solutions, and the dotted lines the WKBJ approximations. Radiative ('rad') and resonant ('res') instabilities are present.

in tangential flow u. We are then left with the problem on the reduced range $0 \leqslant y \leqslant 1$, to solve the differential equation for g in the case of constant shear,

$$\partial_y^2 g = k^2 \varDelta\, g, \quad \varDelta = \varDelta_0 + k^{-2}\varDelta_1, \tag{3.4}$$

$$\varDelta_0 = 1 - F^2(1-y-c)^2, \quad \varDelta_1 = 2(1-y-c)^{-2}, \tag{3.5a,b}$$

subject to

$$g'(0)/g(0) = (1-c)^{-1}, \quad g'(1)/g(1) = -c^{-1} - k\sqrt{1-F^2c^2} \quad \text{or} \quad -c^{-1} \pm \mathrm{i}k\sqrt{F^2c^2-1}. \tag{3.6a,b}$$

3.1. *Numerical results*

The eigenvalue problem was solved using a shooting code for (2.13) and the eigenmode branches, that is c_r and c_i (solid curves), are shown in figure 3 as functions of k. When a mode is neutral, $c_i = 0$, any critical point y_c lies on the real axis and makes the differential equation singular there. Although the singularity is easily treated analytically for this piecewise linear profile, the shooting has to be done on a path in the complex plane, for example a parabolic arc from zero to one above or below y_c.

This figure reproduces results of Satomura (1981) and shows a variety of eigenmode branches. We turn first to frequencies plotted in figure 3(*a*). Ignoring for a moment resonances near to branch crossings, we have two different types of branches. There is a single branch (somewhat broken up by resonances) with $\mathrm{d}c_r/\mathrm{d}k < 0$, tending to the horizontal axis as $k \to \infty$: we refer to these modes as 'limit modes (LM)'. These modes are localised on the discontinuity at $y = 1$ and continue to exist in the incompressible limit $F \to 0$; these can be interpreted as Rayleigh waves or edge modes on a piecewise linear profile (e.g. Sutherland 2010). There is also a sequence of branches with increasing frequency as $k \to \infty$, $\mathrm{d}c_r/\mathrm{d}k > 0$, and we refer to these

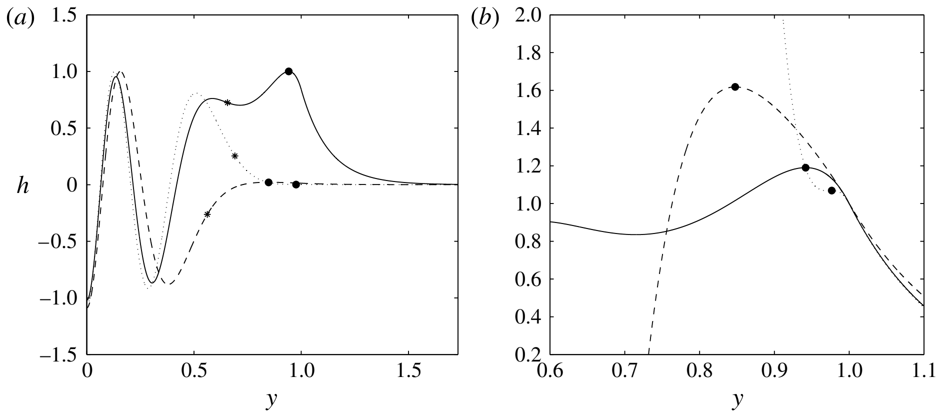

FIGURE 4. Structure of the three neutral modes for the piecewise linear profile (3.1) with $k=8$, (*a*) scaled by their maximum amplitude, and (*b*) view zoomed in near the critical points with solutions scaled by their values at $y=1$. The (real) $h(y)$ field is plotted against y for the LM with $c=0.0581$ (solid), the third discrete mode for $c=0.152$ (dashed), and fourth discrete mode for $c=0.0235$ (dotted). The positions of critical points y_c (•) are shown in (*a*,*b*) and turning points $y_t \equiv y_{t1}$ (∗) in (*a*) only.

as SG wave modes, since branches show increasing numbers of oscillations in the fluid domain adjacent to the boundary $y=0$. We observe all three classes of modes discussed at the end of § 2, leaving aside resonances at branch crossings.

First, for $c_r \in (-F^{-1}, 0)$ the branches of SGM are all neutral and there is no critical point: these modes belong to class A. Secondly, for $c_r \in (0, F^{-1})$ and away from branch crossings, the branches of SGM are again neutral, and so is the limit branch: these fall in class B. In this case there is a critical point y_c in the domain (with $0 \leqslant y_c < 1$) but this does not lead to damping or destabilisation of the mode. This is a consequence of the piecewise linear profile: the background potential vorticity gradient Q' is zero at the critical point, and there is none of the feedback from vorticity transport in a critical layer. Linked to this, a Frobenius development of (3.4), (3.5) near to the critical point y_c gives a simple pole in $g(y)$ and a non-singular height field $h(y)$ (Satomura 1981). This means that numerical eigenvalues can be obtained equally from shooting above or below y_c in the complex plane.

For $c_r \in (F^{-1}, 1-F^{-1})$ the SGM are radiative and fall in class C. They have a positive or negative growth rate which pushes the critical point y_c off the real axis. In figure 3(*b*) they correspond to long, low elongated 'bubbles' with growth rates of $O(10^{-3})$ or less; however only the first can be seen, clinging to the axis for $k>2.7$, labelled 'rad'. For the growing radiative mode, the boundary condition (3.6) is used with the sign chosen to correspond to an outgoing wave as $y \to \infty$. However for the decaying mode it is an incoming wave with the opposite sign of the square root taken in (3.6). Thus it is only the upper portion of the bubble which corresponds to the physically important case of RI.

The structure of three neutral modes, namely LM, and third and fourth SGM, is shown in figure 4 for $k=8$. The curves were obtained by integrating along the real axis on both sides of the critical point, using the eigenvalue c first obtained by means of shooting along a complex path. Note that the SGM (dashed and dotted lines) are oscillatory up to their turning points y_{t1} (∗) and then die away rapidly to very low amplitude at their critical points y_c (•). On the other hand the LM (solid line) has a peak at its critical point y_c; although it decays only a little for $y < y_c$, for large k this branch of solutions is represented at leading order by evanescent decay as y is reduced below y_c. We will pick up this structure in the WKBJ analysis below.

Where the branches for c_r cross in figure 3(*a*), the corresponding modes become resonant, giving the tall, narrow bubbles of instability labelled 'res' in figure 3(*b*). There are two solutions with positive or negative growth rate and each solution corresponds to a mixture of the two individual non-resonant modes. For these resonant bubbles, the two solutions with opposite growth rates can again be obtained by shooting above or below the critical point y_c, which is now pushed off the real axis.

3.2. *WKBJ theory for surface gravity modes*

We now turn to analysis of the features seen in figure 3, and in the remainder of this section are interested in modes in class B, with wave speed $c_r \in (0, F^{-1})$. Our aim is to describe limit and SGM using WKBJ analysis for large k (e.g. Bender & Orszag 1978) and to give a description of the resonances that occur when branches cross. At the outset, in this subsection and § 3.3 we seek the two separate families of SGM, localised near the boundary, and LMs, localised near the discontinuity, as separate branches by requiring exponential decay in the evanescent region that separates them. We then investigate resonant interactions by connecting solutions through the evanescent region, giving effects exponentially small in k as $k \to \infty$, in § 3.4.

Supposing first that $c = c_r$ is real, we have a single real turning point y_t and a real critical point y_c, with $0 < y_t < y_c < 1$. We divide space into three regions, defined loosely as region I, $0 \leqslant y < y_t$, region II $y_t < y < y_c$ and region III $y \simeq y_c$. We start in region I with the standard oscillatory form of the WKBJ solution in (2.18). For large k the solution satisfying the boundary condition at $y = 0$ in (3.6), which at leading order in k simply amounts to $g'(0) = O(1) \ll k$, is

$$g_I = A(-\Delta)^{-1/4} \cos\left(k \int_0^y \sqrt{-\Delta}\, \mathrm{d}y\right). \tag{3.7}$$

This is valid in region I, in which $\Delta \simeq \Delta_0 < 0$, and may be rewritten as

$$g_I = A(-\Delta)^{-1/4} \sin\left(k \int_y^{y_t} \sqrt{-\Delta}\, \mathrm{d}y - \Phi + \pi/4\right), \tag{3.8}$$

with a phase defined by

$$\Phi = k \int_0^{y_t} \sqrt{-\Delta}\, \mathrm{d}y - \pi/4. \tag{3.9}$$

We move to region II where $\Delta_0 > 0$ and suppose that we are sufficiently far from the critical point that the WKBJ approximation remains valid. We may write this solution in the form

$$g_{II} = \Delta^{-1/4}\left[C \exp\left(k \int_{y_t}^y \sqrt{\Delta}\, \mathrm{d}y\right) + D \exp\left(-k \int_{y_t}^y \sqrt{\Delta}\, \mathrm{d}y\right)\right]. \tag{3.10}$$

To find branches of solutions we now ignore the effect of the critical point and just require evanescent solutions in region II. In fact the presence of a critical point can have a weak destabilising effect, but only near to mode crossings as we will discuss below. A standard argument (e.g. Bender & Orszag 1978) involves matching the oscillatory solution (3.7) to the evanescent solution with $C=0$ (via an Airy function approximation) and gives the leading-order dispersion relation for these modes as $\Phi = n\pi$ or

$$k\int_0^{y_t} \sqrt{-\Delta}\,\mathrm{d}y = n\pi + \pi/4. \tag{3.11}$$

Away from any critical point we may approximate Δ by Δ_0 up to corrections of order k^{-2}. Evaluating the integral then gives the dispersion relation explicitly as

$$\tfrac{1}{2}kF^{-1}\left[F(1-c)\sqrt{F^2(1-c)^2-1} - \cosh^{-1}(F(1-c))\right] = n\pi + \pi/4. \tag{3.12}$$

This approximation (dotted lines) gives the SG branches depicted in figure 3(a) with excellent agreement for large k. The two SGM shown in figure 4 (dotted and dash curves) have the correct qualitative structure, in particular the exponential decay beyond the turning points ($*$).

3.3. *Asymptotic theory for limit modes*

The branch of LMs which approaches the horizontal axis of figure 3(a) has its origin elsewhere. As seen in figure 4 such a mode (solid curve) has a peak close to $y=1$ and from figure 3, c is real (except at the mode crossings), positive and tends to zero for large k. Experimentation suggests that $c=c_r=O(k^{-1})$ is the appropriate scaling and we take this as a working assumption. In this case a critical point, with $U(y_c)=c$, given by $y_c=1-c$ approaches $y=1$ as k tends to infinity and we seek an eigenmode localised there. We call this region III, which is defined formally by $y-y_c \ll k^{-1/2}$ and includes the point $y=1$. In region III we can no longer ignore Δ_1 in (3.4), (3.5) but it is now legitimate to approximate Δ_0, so that

$$\Delta \simeq 1 + k^{-2}\Delta_1 = 1 + 2k^{-2}(y-y_c)^{-2}, \tag{3.13}$$

and then the resulting differential equation

$$\partial_y^2 g = [k^2 + 2(y-y_c)^{-2}]g \tag{3.14}$$

transforms to a Whittaker equation for $w=2k(y-y_c)$,

$$\partial_w^2 g + (-\tfrac{1}{4} - 2w^{-2})g = 0. \tag{3.15}$$

This equation is discussed in § 13.14 of Olver (2010) and in its standard form ((5.7) below) has two parameters which here take the values $\kappa=0$, $\mu=3/2$. The solution may be expressed as

$$g_{III} = EW_{0,3/2}(w) + GW_{0,3/2}(-w), \tag{3.16}$$

or explicitly

$$g_{III} = E[1+k^{-1}(y-y_c)^{-1}]\mathrm{e}^{-k(y-y_c)} + G[1-k^{-1}(y-y_c)^{-1}]\mathrm{e}^{k(y-y_c)}. \tag{3.17}$$

It may be checked that this solution matches to the exponential WKBJ solution (3.10) in region II. Note that the solution g_{III} has a simple pole at $y=y_c$ whereas the corresponding height field h (2.15) is regular there. We will later see that the situation becomes more complicated for profiles where $Q' = -U''$ is non-zero at the critical point and the Whittaker functions gain branch cuts.

We can now impose the boundary condition (3.6) at $y = 1$ on the solution (3.17), and we may neglect F^2c^2 on the right-hand side as $c = O(k^{-1})$, leaving us to require only $g'(1)/g(1) = -c^{-1} - k$. Some rearrangement gives

$$E/G = (1 - 2kc)\mathrm{e}^{2kc}. \tag{3.18}$$

Finally, for a solution localised about the critical point we require exponential decay as y decreases below y_c, in other words $E = 0$, leaving the branch described by the approximation

$$c = (2k)^{-1}, \tag{3.19}$$

valid for large k, independent of Froude number. This approximation is shown in figure 3(a) (dotted curve) and shows good agreement with increasing k. These LMs have a peak localised close to $y = 1$ for large k, as illustrated in figure 4 (solid curve), and so can be thought of as driven by the jump in potential vorticity Q at $y = 1$, much like a normal mode on a Rankine vortex in the analogous problem in plane polar geometry (Ford 1994).

3.4. *WKBJ theory for resonances*

We have identified a set of branches of SGM, trapped between $y = 0$ and $y = y_t$ and a branch of LMs, localised at a critical point y_c close to the boundary $y = 1$ of the shear flow. We observe resonances between these modes where the branches cross in figure 3, and now sketch the analysis of these following Knessl & Keller (1995). This involves keeping track of both exponential components of the evanescent WKBJ solution (3.10) in $y_t < y < y_c$, even though we neglect terms of order k^{-1} in each one; we need to keep the two independent solutions at leading order (no matter how weak one is) to capture an effect that is exponentially small as $k \to \infty$ (Shepard 1983).

Matching the WKBJ solutions (3.8) and (3.10) across the turning point y_t gives

$$C/D = -2 \tan \varPhi \tag{3.20}$$

and matching the solution (3.17) for $y < y_c$ to (3.10) for $y > y_t$ yields (omitting details),

$$G = C \exp(\tfrac{1}{4}\pi k F^{-1}), \quad E = D \exp(-\tfrac{1}{4}\pi k F^{-1}). \tag{3.21a,b}$$

Using also (3.18), the resulting dispersion relation is found to be

$$(kc - \tfrac{1}{2}) \tan \varPhi = \tfrac{1}{4} \exp(-\tfrac{1}{2}\pi k F^{-1} - 2kc). \tag{3.22}$$

The right-hand side is exponentially small for large k and, if neglected, we regain the SG and limit branches we already have, namely (3.11) and (3.19). We work near to a branch crossing, labelled by n, where simultaneously both conditions are satisfied,

$$\varPhi_n = n\pi, \quad k_n c_n = \tfrac{1}{2}, \tag{3.23a,b}$$

and set $c = c_n + \delta c$, $k = k_n + \delta k$. The dispersion relation (3.22) takes the form

$$(\delta c + \alpha\, \delta k)(\delta c + \beta\, \delta k) + \gamma = 0 \tag{3.24}$$

to leading order in δc, δk, where the coefficients are

$$\alpha = c_n k_n^{-1} = \tfrac{1}{2} k_n^{-2}, \quad \beta = -k_n^{-2}(F^2-1)^{-1/2}(n\pi + \pi/4), \tag{3.25a,b}$$

$$\gamma = \tfrac{1}{4} k_n^{-2}(F^2-1)^{-1/2} \exp(-\tfrac{1}{2}\pi k_n F^{-1} - 1). \tag{3.26}$$

The approximate dispersion relation (3.24) is solved as

$$2\delta c = -(\alpha+\beta)\delta k \pm \sqrt{(\alpha-\beta)^2 \delta k^2 - 4\gamma}. \tag{3.27}$$

Now $\gamma > 0$ as $F > 1$ for class B modes (see figure 1) and so for small δk we obtain a pair of complex roots and instability. We have an interval about k_n given by $|\delta k| < 2\sqrt{\gamma}|\alpha-\beta|^{-1}$ in which we have complex roots. The maximum growth rate will occur at $\delta k = 0$ and is given by $\delta c = \pm \mathrm{i}\sqrt{\gamma}$. The theoretical calculation is plotted on figure 3(*b*) (dotted curve), with the resonance bubbles centred on the crossings (k_n, c_n) of the approximate branches in (3.23). We observe improving agreement as k increases.

The resonant interaction presented in this part is very similar to the resonant instability of a purely linear shear flow, with $Q' = -U'' = 0$, between two walls. In this case two neutral SGM, with the same frequencies and localised on opposite walls interact (Balmforth 1999). The resulting instability has been explained as a coupling between two SG waves with opposite signs of wave action, energy or momentum (Hayashi & Young 1987), or as an over-reflection process, or as two waves propagating energy in opposite directions (as they have opposite group velocities) with the region of the critical point acting as an energy source (Le Dizès & Billant 2009).

To link this case of a linear profile with the piecewise linear profile of this section and Satomura (1981), note first that the existence of the LM is a result of the discontinuity of Q at $y = 1$. Its existence as a neutral mode is also linked to the finite limit $U(\infty)$. If $U(y)$ is unbounded as $y \to \infty$ then all modes radiate at infinity, and none of the modes would be neutral. Secondly arguments based on coupling of modes with opposite signs of wave momentum cannot be applied here. The discontinuity in Q also gives a contribution to the rate of change of M in (2.12) through a delta-function source of q. Thus M is no longer conserved and wave momentum can now be extracted from the background shear flow. Whereas for a strictly linear profile, with $Q = 0$ everywhere, any unstable mode must have zero M and so can only arise from the resonance between modes with positive and negative M, for the piecewise linear profile this is no longer the case. Both SGM and LM have negative M, as discussed below.

4. Nonlinear profiles

In our analysis of the LMs in the piecewise linear profiles in the previous section, the gradient of potential vorticity at the critical point is zero, and this is a key simplification. In this section we allow nonlinear shear in the region $0 < y < 1$, using members of the family of profiles

$$U_1(y) = \begin{cases} (1-\mu y)(1-y) & (0 \leqslant y \leqslant 1), \\ 0 & (y > 1), \end{cases} \tag{4.1}$$

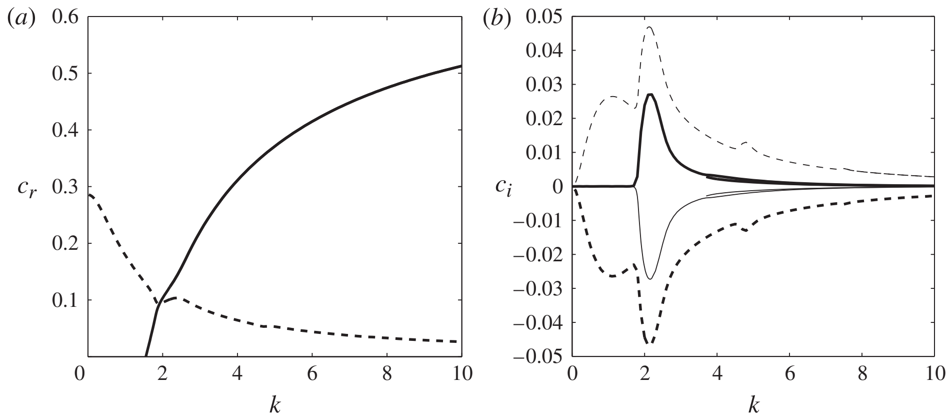

FIGURE 5. First SGM (thick solid) and limit quasi-mode (LQM) (thick dashed) for the profile U_1 in (4.1) with $\mu = 0.5$: (*a*) c_r and (*b*) c_i. The thin curves in (*b*) result from integrating below the critical point y_c in the complex y-plane.

depicted in figure 2(*a*). The parameter μ gives the potential vorticity gradient and the curvature of the profile with $U'' = -Q' = 2\mu$, and $\mu = 0$ is the previous piecewise linear case. We consider how frequencies c_r and growth rates c_i are changed as $|\mu|$ is increased from zero. Note that the situation has some similarities with that discussed by Balmforth (1999) for a finite channel, but in that case the symmetry of the channel increases the number of modes. We focus on just the first SGM and the LM; further branches of SGM show similar behaviour.

Referring to the classification of § 2.2, modes in class A do not have a critical point and so remain neutral. However this slight change in the profile results in significant effects on modes in classes B and C. First the critical point is slightly moved in the complex plane. For radiative modes $c_i > 0$ already and so this is just a modification to the growth rate. However for the previously neutral modes there is the appearance of a small imaginary part c_i, and this is the origin of CLI.

Secondly, the eigenvalue problem now has different solutions depending on whether the path of integration is taken above or below a critical point of the governing differential equation in the complex plane. When $\mu \neq 0$, the U'' term of Δ_1 in (2.19) is non-zero, and the height field h at the critical point is singular, generally gaining a branch cut. For this reason the two branches of solutions for $\mu = 0$ in figure 3(*b*) become four branches, shown in figure 5 for $\mu > 0$ and figure 6 for $\mu < 0$. Solid lines give the modes and dashed lines the QMs. Thick lines correspond to integrating above the critical point and thin lines below, giving complex-conjugate values of c and so stable/unstable pairs. The resonant bubbles from figure 3 leave a clear imprint in each case, but to explain the overall structure it is more helpful to focus on a case in between such bubbles, where the original $\mu = 0$ modes are neutral in figure 3.

The effect of introducing a background potential vorticity gradient is then shown schematically for class B modes in figure 7 which indicates the locations of eigenvalues for c and corresponding values of y_c in the complex c-plane (*a*–*c*) and complex y-plane (*d*–*f*). In figure 7(*a*,*d*) the two neutral modes (LM, SGM) are depicted for $\mu = 0$ (away from resonance and with, say, $k > 2$ for definiteness). Now for $\mu > 0$ an integration path is taken well (*b*,*e*) above or (*c*,*f*) below the complex y-axis and the two neutral modes in (*a*,*d*) move off the real axis; the sense in which

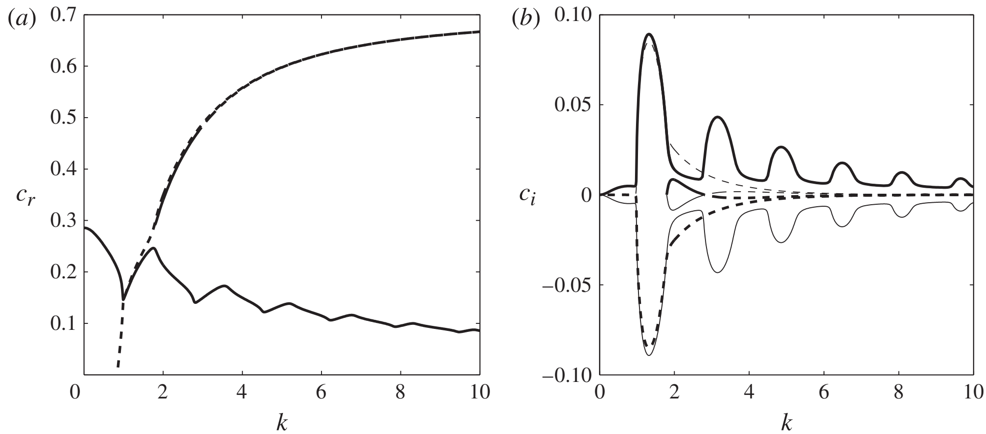

FIGURE 6. First surface gravity quasi-mode (SGQM) (thick dashed) and LM (thick solid) for the profile U_1 in (4.1) with $\mu = -1$: (*a*) c_r, and (*b*) c_i. The thin curves in (*b*) result from integrating below the critical point y_c in the complex *y*-plane. The radiative mode for $c_r \in (0.28, 0.47)$ becomes a QM for $c_r \in (0.47, 0.71)$.

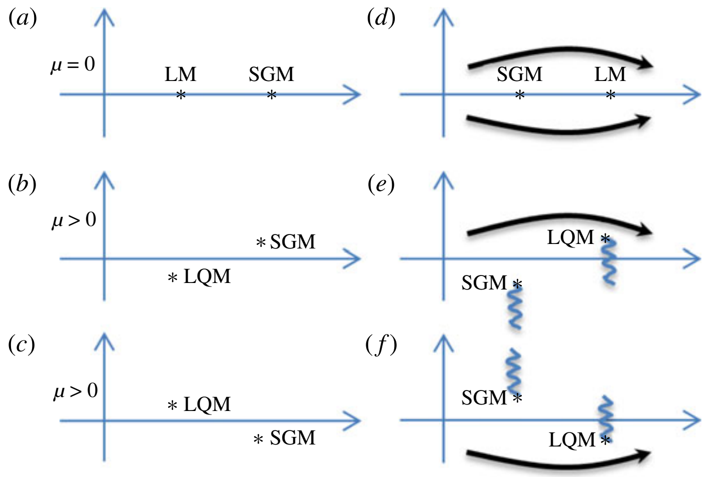

FIGURE 7. (Colour online) Schematic picture of eigenvalues in the complex *c*-plane (*a*–*c*) and critical points y_c in the complex *y*-plane (*d*–*f*) for surface gravity (SG) and limit (L) modes (M) and quasi-modes (QM). (*a*,*d*) $\mu = 0$, (*b*,*e*) $\mu > 0$ with *y*-contour taken above y_c, and (*c*,*f*) $\mu > 0$, with contour taken below y_c. Branch cuts are also indicated.

they are tipped off is opposite in *c*- and *y*-planes since $U'(y) \leqslant 0$ for this and other flows we consider. Because the solutions gain a branch point at y_c and a branch cut in the *y*-plane, the neutral SGM in (*a*,*d*) becomes a pair of normal modes (SGM) in (*b*,*e*) and (*c*,*f*), but the neutral LM becomes a pair of limit quasi-modes (LQM). For $\mu < 0$, the situation is reversed and we gain a pair of SGQM and a LM (not depicted). The two modes and the two QMs have the same value for c_r but have opposite growth rates: see figure 5 for positive μ, and figure 6 for negative μ. Note that in general a solution is called a QM when the critical point y_c lies between the real axis and the complex *y*-path used to obtain it; an attempt to distort the contour to the real axis would encounter the branch cut and so give a discontinuous solution for the physical fields (Briggs *et al.* 1970). This discontinuity would signal the need for a critical layer, in which the vorticity field is sheared to small scales, for a complete description of the time evolution. For a normal mode there is no barrier (i.e. critical point) between distorted contour and the real axis.

We make some further remarks. First the situation is complicated because of the presence of the two branches of continuous spectrum noted in (2.25), (2.26). When a neutral mode for $\mu = 0$ turns into two quasi-modes, these are really on separate Riemann surfaces of the dispersion relation, only apparent by either going through a branch cut of continuous spectrum, or by distorting the y-contour so as to shift this branch cut and so reveal the quasi-mode (Briggs *et al.* 1970). Related to this is the issue of causality. In our discussion so far, both branches of quasi-modes are given on an equal footing, as in Balmforth (1999), to show how solutions of the eigenvalue problem are modified because of the nonlinearity of the profile and how modes are connected to quasi-modes as the parameter μ is taken to pass through zero. However considering an initial value problem using a Laplace transform setting (Briggs *et al.* 1970; Schecter & Montgomery 2004), requires a inversion contour sitting above any singularities in the c-plane. Then, to reveal a quasi-mode on another Riemann sheet, it is necessary to raise the y-contour so as to lower the continuous spectrum in the c-plane (in our flows with $U' \leqslant 0$), as depicted in figure 7. Note that as a Landau pole can be considered as a component of the continuous spectrum, it dominates the full evolution during a transient period before being overtaken by other components that decay only algebraically. This period increases the closer the pole is to the c_r-axis, i.e. the less the quasi-mode is damped; however information about Landau poles is relevant for the evolution of disturbances and processes such as cat's eye formation and mixing, even when the quasi-mode is not weakly damped (Schecter *et al.* 2000; Turner *et al.* 2008).

In any case, only the damped quasi-mode is relevant to the initial value problem and we can discard quasi-modes obtained with a path taken below the y-axis (for example the thin, dashed curves in figures 5(b) and 6(b)). While quasi-mode damping can be considered as a result of fine structure being sheared to finer and finer scales in a critical layer, the possibility of quasi-mode amplification would correspond to indefinitely fine structure being unsheared in the critical layer, at odds with the nature of a (smooth) initial condition. Similar considerations apply to the robustness of modes in the presence of weak viscosity (Lin 1945; Balmforth 1999), and we have confirmed this by time-stepping (2.1) (with an additional viscous term). From here onwards we only consider the physical solutions obtained with the path taken above critical points in the y-plane (thick curves). With this, for class B modes, $c_r \in (0, F^{-1})$, the mode and the quasi-mode have independent dispersion relations: profiles with $\mu > 0$ have amplified SGM and damped LQM; for $\mu < 0$ it is the opposite way round.

Introducing nonlinearity $\mu \neq 0$ has a similar effect on radiative modes as on a SGM: $\mu > 0$ leads to amplification and $\mu < 0$ leads to damping. Note that, as for class B modes, there are again two solutions for a given c_r in the interval of class C modes. In fact the solution for $c_i > 0$ is obtained with the boundary condition of an outgoing wave and the other with $c_i < 0$ with that of an incoming wave. For small μ the growing outgoing solution is a mode and the damped incoming solution a quasi-mode. If μ is large, positive or negative, the sign of c_i can change and hence the mode change to quasi-mode or conversely. This can be seen in figure 5 and in figure 6 for $c_r > 0.47$. Note that in figure 5 the growing mode associated with an incoming wave boundary condition is not physically relevant.

We can summarize the effect of weak nonlinearity of the profile according to the range of wave speed c_r. For class B, neutral modes become a mode/quasi-mode pair with two very different structures and frequencies. For class C, radiative modes become a mode/quasi-mode pair with very close frequencies corresponding to a growing radiative mode with an outgoing wave and a damped quasi-mode with an incoming wave. An approximate formula for CLI of a smooth flow may be obtained by integrating (2.12) along the real y-axis (Kubokawa 1985; Balmforth 1999) linking the growth rate c_i to the wave momentum M and the characteristics of the flow at the critical point,

$$|c_i| = \frac{\pi Q_c' |v_c|^2}{2k^2 M |U_c'|}. \tag{4.2}$$

These modes split into growing/decaying pairs or disappear entirely depending on whether Q_c'/M is positive or negative. When the modes disappear, for $Q_c'/M < 0$, they become quasi-modes and the left-hand side of (4.2) is to be replaced by $-|c_i|$, from integrating on the other side of the critical point in the y-plane (Balmforth 1999). In fact for the profiles we study, the limit and SGM both have both negative momentum M and the same sign for $Q_c' = -2\mu$. However they appear and disappear for opposite values of μ, in apparent contradiction with (4.2). The reason is that this formula does not apply to the profiles in (4.1) because U' is discontinuous at $y = 1$. Incorporating a term $Q'(y) = Q_d \delta(y - y_d)$ in the vorticity gradient (see appendix A) gives instead

$$|c_i| = \frac{\pi Q_c' |v_c|^2}{2k^2 |U_c'|} \left(M - \frac{Q_d |v_d|^2}{2k^2 c_r^2} \right)^{-1}, \tag{4.3}$$

and predictions from this formula are in line with our results. So, for example, the $\mu = 0$ SGM is weak near the discontinuity (i.e. in the evanescent region), has $|v_d|$ small, and so (4.3) becomes the same as (4.2), this mode disappearing for $\mu < 0$. For the LM, localised near the discontinuity, $|v_d|$ is larger giving a key sign change between the right-hand sides of (4.2) and (4.3).

5. Smooth profiles

We have determined the structure and growth rates of disturbances to the piecewise linear profile (3.1) of Satomura (1981), and how introducing curvature to the flow profile leads to CLI and the creation of quasi-modes. However (unless $\mu = 1$) these profiles have a discontinuity in derivative $U'(y)$ at $y = 1$ which has two implications. First the LM discussed above and given explicitly by (3.17) for $\mu = 0$ is localised near to the discontinuity of $U'(y)$. Smoothing the profile will have a big impact on this mode and it may disappear entirely. Secondly, it is is difficult to present an analysis because of having to impose the boundary condition (3.6) at $y = 1$: this point sits in the region where the solution is described by Whittaker functions and imposing a boundary condition here does not lead to useful or explicit formulae. For these reasons we consider profiles that have continuous $U'(y)$ in this section. The focus is on profiles with finite limiting velocity $U(\infty)$ as $y \to \infty$ in § 5.1 and unbounded profiles in § 5.3.

5.1. *Profiles with bounded velocity*

We consider the piecewise profile $U_1(y)$ in (4.1) with $\mu = 1$, and the smooth profiles,

$$U_2(y) = 1 - \tanh y, \quad U_3(y) = (1 + y)^{-1}. \tag{5.1a,b}$$

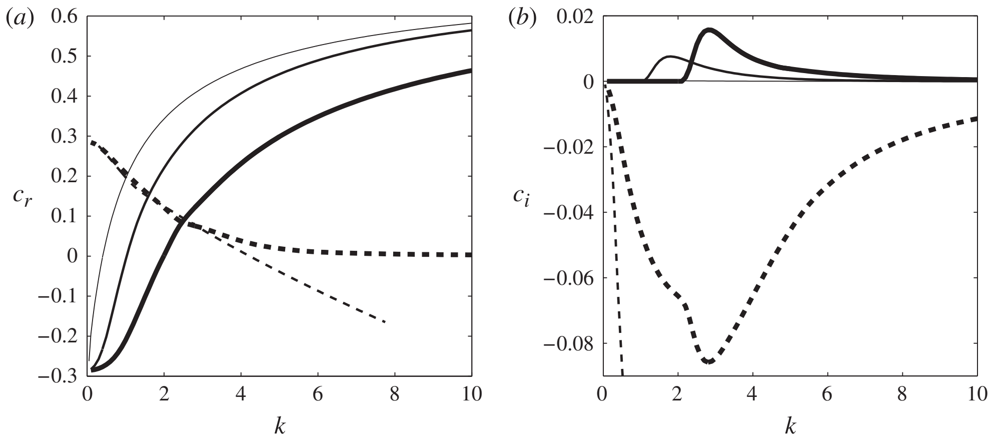

FIGURE 8. CLI: (*a*) c_r and (*b*) c_i for first SGM (solid) and limit quasi-mode (LQM) (dashed) for $F = 3.5$ and profiles U_1, $\mu = 1$ in (4.1) (thickest), U_2 (thick) and U_3 (thin) in (5.1). Note that the thinnest dashed lines are absent (see text).

U_1, U_2 and U_3 tend to zero increasingly slowly for large y; see figure 2(*b*). As in Riedinger *et al.* (2010*a*) results were obtained using the spectral code on a complex path defined by the variable $\arg y = \pi/10$. Results were checked afterwards using a shooting code. The phase velocity c_r and growth rate c_i are given for the unstable mode and the limit quasi-mode in figure 8 for the three profiles. Using the spectral code on this complex path has the effect of lowering both branches of continuous spectrum (2.25), (2.26) in the c-plane, and revealing quasi-mode eigenvalues (Riedinger *et al.* 2010*a*). The integration path is always taken above critical points, so imposing causality or effects of weak viscosity.

Looking first at the curves for the piecewise profile U_1 in figure 8 (which can also be compared with figure 5 for $\mu = 0.5$) the gravity wave mode (thickest solid) becomes unstable as soon as c_r becomes positive, when the critical layer is present for $k > 1.99$. The maximum $c_i = 0.0157$ is obtained for $k \simeq 2.8$ a little after the crossing of c_r branches in figure 8(*a*) at $k \simeq 2.475$. The c_i branch for the limit quasi-mode in figure 8(*b*) (thick dashed) shows a similar but inverted bump, i.e. a trough, for these values of k, corresponding to increased damping. Returning to the SGM, there is now no obvious distinction between this and the resonance which we had in figure 3(*b*) and this allows us to draw a new interpretation of the CLI in these smoother profiles with $U'' \neq 0$ as the remnant or 'ghost' of the interaction between the SGM and the LM in the piecewise linear profile. Informally, in the latter case all of the U'' is concentrated in a delta function at $y = 1$, and the unstable resonance with the resulting LM is analogous to the CLI when the non-zero U'' is distributed, over the critical layer.

The U_2 and U_3 profiles are entirely smooth, but tend to zero exponentially and algebraically, respectively. For U_2 the curves for c_r (thick) in figure 8(*a*) are similar to those for U_1, but the growth rate for the limit quasi-mode figure 8(*b*) (thick dashed) becomes increasingly negative as k is increased, and so is strongly damped. The SGM (thick solid) is amplified, but more weakly now. For U_3 these effects are more pronounced: the SGM is amplified (thin solid) but cannot be seen on the figure as the maximum of c_i is 1.6×10^{-4}. We have not been able to obtain the quasi-mode for U_3, indicated by the absence of thin dashed curves in the figure; indeed the critical point that must be circumnavigated is expected to be far above the real axis.

In summary, the smoother the profile, i.e. the smaller is U'', the lower is the CLI growth rate for the SGM and the stronger is the damping of the limit quasi-mode, to the point where it cannot easily be detected numerically.

5.2. *WKBJ theory for critical layer instability*

We now develop a theoretical framework for the above numerical results in the case of smooth profiles. We work on $0 \leqslant y \leqslant \infty$ and return to the full set of equations (2.16)–(2.19) for any smooth profile $U(y)$, with boundary conditions (2.23) and (2.24). We assume we have a single turning point y_t and a critical point y_c with $0 < y_t < y_c < \infty$. The difficulty for a nonlinear profile is the more complicated form of Δ_1 in (2.19) which generally gives a branch cut in the solution at a critical point y_c if U'' is non-zero there, i.e. $Q'_c = -U''_c \neq 0$.

In line with our discussion in § 3.2, we specify region I as $0 \leqslant y < y_t$, region II as $y_t < y < y_c$, region III as a neighbourhood of y_c and region IV as $y > y_c$. In regions I and II we have the WKBJ solutions (3.7) and (3.10) exactly as before and these are connected through the turning point via (3.20). In region IV we have an evanescent wave

$$g_{IV} \propto \Delta^{-1/4} \exp\left(-k \int^y \sqrt{\Delta}\, \mathrm{d}y\right). \tag{5.2}$$

The key problem is to link up the solutions in regions IV and II across the critical point. As before we consider region III, defined formally by $|y - y_c| \ll k^{-1/2}$, and approximate

$$\Delta \simeq 1 + k^{-2}\Delta_1. \tag{5.3}$$

Using the smoothness of the profile and a Taylor series expansion, the term Δ_1 has the following singular component as y_c as approached:

$$\Delta_1 = 2\tilde{y}^{-2} + (U''_c/U'_c)\tilde{y}^{-1} + \cdots, \tag{5.4}$$

where we have set $\tilde{y} = y - y_c$ for convenience. Thus in region III (2.16) for g becomes at leading order

$$\partial_y^2 g = [k^2 + (U''_c/U'_c)\tilde{y}^{-1} + 2\tilde{y}^{-2}]g, \tag{5.5}$$

or, with

$$w = 2k\tilde{y}, \quad \kappa = -U''_c/2kU'_c, \quad \mu = 3/2, \tag{5.6a–c}$$

we obtain the standard form of the Whittaker equation (Olver 2010)

$$\partial_w^2 g + [-\tfrac{1}{4} + \kappa w^{-1} + (\tfrac{1}{4} - \mu^2)w^{-2}]g = 0. \tag{5.7}$$

The general solution may be written

$$g = EW_{\kappa,3/2}(2k\tilde{y}) + GW_{-\kappa,\mu}(\mathrm{e}^{\pm \mathrm{i}\pi}2k\tilde{y}), \tag{5.8}$$

using (13.14(v)) of Olver (2010). Either sign can be taken, giving different but related branches of the Whittaker function.

For $|z| \to \infty$, Whittaker functions have the dominant asymptotic behaviour

$$W_{\kappa,\mu}(z) \sim \mathrm{e}^{-z/2}z^{\kappa} \quad (-3\pi/2 < \arg z < 3\pi/2) \tag{5.9}$$

(Olver 2010, (13.14.21)) and so in (5.8) we set $G = 0$ to match to evanescent decay in region IV (5.2). The resulting solution in (5.8) also matches to an exponential solution in region II (3.10) with $C=0$ and this gives the leading-order structure of a neutrally stable mode. However to pick up the effect of the critical layer on the stability of the mode we need also to keep track of the subdominant component of the Whittaker function. Although this is an exponentially small contribution, by stabilising or destabilising the mode, this pushes c below the real axis, $c_i<0$, or above, $c_i>0$. Similarly y_c is pushed below the real axis if $U'_c c_i<0$ or above if $U'_c c_i>0$. As we integrate above the critical point for reasons of causality and $U'\leqslant 0$, we obtain a normal mode if $c_i>0$ and a quasi-mode if $c_i<0$ in what follows (cf. figure 7).

We relegate the details to appendix B and give the connection formula, from region IV to region II above the critical point in region III, written in terms of $\tilde{y}$:

$$\mathrm{e}^{-k\tilde{y}}(2k\tilde{y})^{\kappa} \longrightarrow \mathrm{e}^{-k\tilde{y}}(-2k\tilde{y})^{\kappa}\mathrm{e}^{\mathrm{i}\pi\kappa}+\mathrm{i}\pi\kappa\,\mathrm{e}^{k\tilde{y}}(-2k\tilde{y})^{-\kappa}\mathrm{e}^{\mathrm{i}\pi\kappa}. \tag{5.10}$$

This indicates that (5.8) for $\tilde{y}>0$ (and $G=0$) connects to

$$g=E\exp[-k\tilde{y}+\kappa\log(-2k\tilde{y})+\mathrm{i}\pi\kappa]+\mathrm{i}\pi\kappa E\exp[k\tilde{y}-\kappa\log(-2k\tilde{y})+\mathrm{i}\pi\kappa], \tag{5.11}$$

which includes both the dominant and subdominant components, valid for $\tilde{y}<0$.

The approximation (5.11) needs to be matched to (3.10) and we do this first quickly and then more carefully. We let $\tilde{y}<0$ be in an overlap region $k^{-1}\ll\tilde{y}\ll k^{-1/2}$ where both the WKBJ form (3.10) and the Whittaker function form (5.11) are valid. In (3.10) we approximate $\varDelta$ by $\varDelta_0$ and evaluate

$$I_1\equiv k\int_{y_t}^{y}\sqrt{\varDelta}\,\mathrm{d}y\simeq k\int_{y_t}^{y}\sqrt{\varDelta_0}\,\mathrm{d}y=V_{tc}-k\int_{y}^{y_c}\sqrt{\varDelta_0}\,\mathrm{d}y\simeq V_{tc}+k\tilde{y}, \tag{5.12}$$

where

$$V_{tc}=k\int_{y_t}^{y_c}\sqrt{\varDelta_0}\,\mathrm{d}y. \tag{5.13}$$

Comparing the leading-order k terms (3.10) and (5.12) with (5.11) yields

$$C\mathrm{e}^{V_{tc}}=\mathrm{i}\pi\kappa E,\quad D\mathrm{e}^{-V_{tc}}=E, \tag{5.14a,b}$$

which with (3.20) gives

$$\tan\varPhi=-\tfrac{1}{2}\mathrm{i}\pi\kappa\mathrm{e}^{-2V_{tc}}. \tag{5.15}$$

This corresponds to a shift in the complex wave speed c, with

$$\tan(\varPhi+\delta\varPhi)\simeq\delta\varPhi=\frac{\partial\varPhi}{\partial c}\delta c,\quad \frac{\partial\varPhi}{\partial c}\simeq -F^2k\int_0^{y_t}(U-c)(-\varDelta_0)^{-1/2}\,\mathrm{d}y. \tag{5.16a,b}$$

The result is a non-zero leading-order value of c_i,

$$c_i=-\tfrac{1}{2}\pi\kappa\mathrm{e}^{-2V_{tc}}(\partial\varPhi/\partial c)^{-1}. \tag{5.17}$$

This formula derived by WKBJ theory is equivalent to (4.2) derived by considering the evolution of wave momentum, as discussed in appendix A.

In matching the solutions in (3.10) and (5.11) we ignored the prefactors and concentrated on the exponential parts to obtain (5.14). Further analysis in appendix C confirms that this is correct at leading order, but also gives a better connection formula including a term in $k^{-1}\log k$, which is the above with V_{tc} replaced by

$$V'_{tc}=V_{tc}+\kappa\int_{y_t}^{y_c}\tilde{y}^{-1}(1-\varDelta_0^{-1/2})\,\mathrm{d}y+\kappa\log[2k(y_c-y_t)]. \tag{5.18}$$

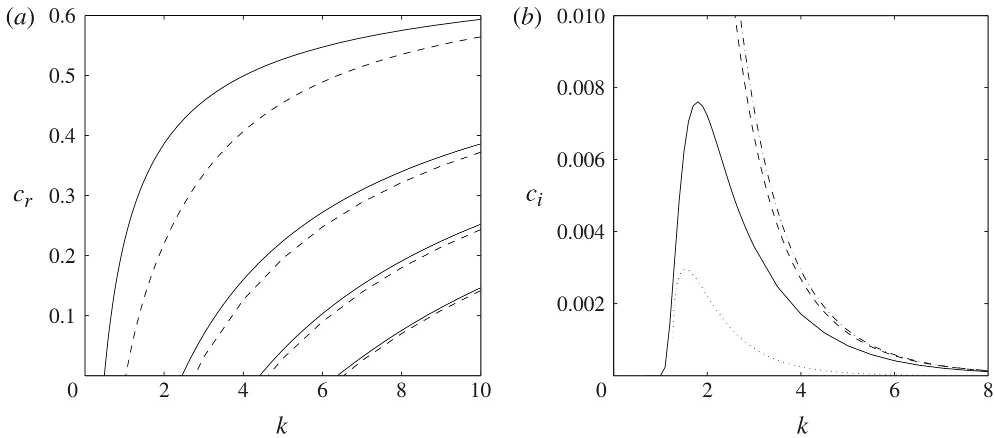

FIGURE 9. Comparison between numerical results (solid) and WKBJ theory for the profile $U_3 = 1 - \tanh(y)$. (*a*) Frequency c_r with formula (3.11) (dashed) for the first four SG wave branches, and (*b*) the growth rate c_i for the first branch and the critical layer term using (5.18) (dashed), and the radiative term using (5.22) (dotted), and combined effects (5.23) (dash–dotted).

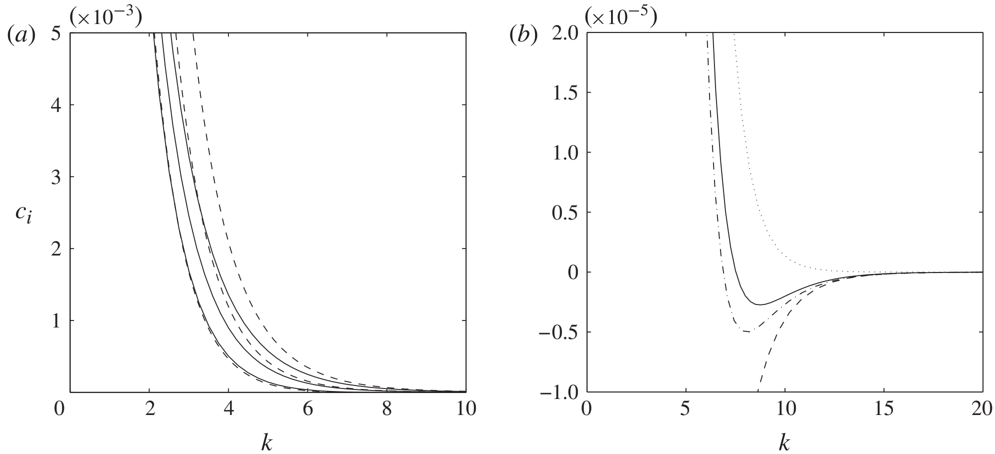

FIGURE 10. Effect of potential vorticity gradient on radiative modes: (*a*) growth rate c_i for U_4 (middle curves), U_5 (right-hand curves), and U_6 (left-hand curves) with numerical results (solid) and formula (5.23) (dashed), and (*b*) close-up view for the profile U_6, with amplifying radiative term (5.22) (dotted), damping critical layer term (5.17) (dashed) and combined effects, (5.23) (dash–dotted).

Figure 9 shows a comparison between numerical and analytical results for U_3, showing gravity wave mode branches (but with no LM present – see figure 8). Notably, in figure 9(*b*) there is good agreement between the growth rate obtained from (5.18) (dash) and the numerical result (solid), especially given that k is not very large. We have also checked this agreement, and likewise for figure 10, on plots of $\log |c_i|$ (not shown). As the frequency c_r increases above F^{-1} the mode becomes radiative at large y, and this gives a corrected growth rate (dash-dotted). As this is a small correction here and both curves are consistent with the numerical results, we defer discussion of the combined effects of critical layer and radiation until the next section.

5.3. *Profiles with unbounded velocity*

Finally we consider three profiles in which the velocity is unbounded at infinity: a linear profile and two with opposite signs of U'',

$$U_4 = 1 - y, \tag{5.19}$$
$$U_5 = 1 - y - 0.1 \tanh y \quad (U'' > 0, \kappa > 0), \tag{5.20}$$
$$U_6 = 1 - y + 0.1 \tanh y \quad (U'' < 0, \kappa < 0). \tag{5.21}$$

For these profiles, modes are radiative for all speeds c_r. The first, linear profile was discussed by Knessl & Keller (1995), in terms of reflection and transmission of waves incident from infinity. We will provide a WKBJ formula for the growth rate including the destabilisation due to radiation. The numerical results used for comparison were obtained using the pseudospectral code outlined in § 5.1.

If the presence of a critical point is ignored and the WKBJ expansion matched across the two turning points, the resulting growth rate is

$$c_i = -\tfrac{1}{4}\mathrm{e}^{-2V_{12}}(\partial\Phi/\partial c)^{-1}, \quad V_{12} = k\int_{y_{t1}}^{y_{t2}} \sqrt{\Delta_0}\,\mathrm{d}y. \tag{5.22}$$

For the linear profile U_4, this is the complete formula, as $U_c'' = 0$ and $\kappa = 0$, and comparison with numerics is given in figure 10(*a*) (middle curves). This shows good agreement in this case of outwards propagating radiated waves at infinity (positive group velocity) giving a positive growth rate (noting that $\partial\Phi/\partial c < 0$ for the modes considered).

For the nonlinear profiles U_5 or U_6 with $U_c'' \neq 0$, the effects of radiation and critical layer may be summed within a perturbative expansion, as in Parras & Le Dizès (2010), giving

$$c_i = \left[-\tfrac{1}{2}\pi\kappa\mathrm{e}^{-2V_{tc}'} - \tfrac{1}{4}\mathrm{e}^{-2V_{12}}\right](\partial\Phi/\partial c)^{-1}, \tag{5.23}$$

with V_{tc}' defined in (5.18). The radiative contribution is always positive (for outward waves at infinity), whereas the critical layer term is positive when $U_c'' > 0$ and negative when $U_c'' < 0$. These can be considered the combined effect of the two overlapping branches of continuous spectrum given in (2.25), (2.26). A parallel may also be drawn between our study and a similar result from Parras & Le Dizès (2010) for compressible round jets: U_c'' can have a stabilising or destabilising effect. However note that for stratified vortices, the equivalent of U_c'', the radial derivative of the axial vorticity at the critical point, always has a stabilising effect on the RI (Schecter & Montgomery 2004; Le Dizès & Billant 2009).

For all three profiles U_4, U_5 and U_6, we show in figure 10(*a*) the combined effects of a gradient of potential vorticity and the RI with good agreement as k is increased. For all of these profiles and moderate k the origin of the instability is mainly radiative. However the critical layer contribution tends to zero more slowly than the radiative term and becomes dominant for large k, which corresponds to large speed c_r, when y_c is close to the boundary. To really test the theory developed, the crucial case is when the radiative and critical layer effects have a opposite signs. This is the case for U_6 and we zoom in on the growth rate as a function of k in figure 10(*b*). Here the RI, dominant for moderate k is taken over by critical layer stabilisation at $k = k_0 \simeq 7.52$. The agreement between the numerical results (solid) and the combined formula (dash–dotted) is clear. Below k_0 the branch corresponds to an unstable normal mode, which becomes a stable quasi-mode for $k > k_0$. (Note that unlike in § 4, no radiative quasi-mode associated with an incoming wave at infinity is presented in this section as these grow spatially as $y \to \infty$ and so cannot be obtained with the pseudospectral code.)

We could not find an equivalent of the branch of LMs (or quasi-modes) seen for other profiles with more pronounced curvature, for example branches for U_1 and U_2 in figure 8. These modes are evanescent at infinity and for the present profiles all modes are radiative at infinity. However there seems no reason why one could not have a LM that is evanescent for small y, but as y increases becomes radiative after a turning point. Such modes would be strongly damped though, for profiles with small values of U'' such as U_5 and U_6, as found for U_3. We may also speculate on the existence of radiative wave quasi-modes when $\kappa > 0$ as for the broken profiles with $\mu < 0$ (see figure 6); we have not seen these and suspect that if they exist they must be strongly damped.

6. Conclusion

We have given an analysis of the CLI and RI in shallow-water fluid flows, for a representative Froude number $F = 3.5$ and varying the shape of the base flow velocity profile. We have considered both piecewise (linear and nonlinear) profiles and smooth profiles, as these give different perspectives on stability in a wide range of fluid flows; for example, a piecewise linear profile, although idealised, is a useful model for understanding instabilities in flows on scales greater than that of a concentrated vorticity gradient. Numerical results were obtained for a range of profiles, with growth rates in agreement with WKBJ analysis in the limit of large wavenumber k, and linked to arguments based on evolution of wave momentum. Across regions where all waves are evanescent, effects which are exponentially small in k can damp or destabilise what would otherwise be neutral modes. In this way, a wave-free or 'balanced' shear flow can spontaneously generate waves, that is become imbalanced, through exponentially small effects, a topic recently reviewed in Vanneste (2013).

For a piecewise linear profile (Satomura 1981), instability occurs in the form of a resonance between SG wave modes and a limit (or Rayleigh) mode, whose structure has been determined. In the absence of resonance this LM is neutral, and its presence is not only a result of the discontinuity in the vorticity, but also of the infinite extension of the evanescent domain which follows from a finite limit $U(\infty)$ of the velocity profile. For more general profiles the neutral LM becomes an unstable normal mode or a damped quasi-mode depending on the sign of the gradient of vorticity in the critical layer. The mode remains as a quasi-mode for the hyperbolic tangent profile (5.1) which does not present any discontinuity. For the profile (5.2) with algebraic fall-off, any LM would become strongly damped and we were unable to obtain it. In this case, the SGM remain unstable but the instability becomes much weaker.

Turning now to the smooth profile we find a useful description of CLI of SGM in this case, as the remnant of the resonance between such modes and the LM in the piecewise case. In both cases it is the presence of vorticity gradients (a delta function at the discontinuity in the piecewise case) that is linked to the destabilisation of the SGM. The description of CLI as the remnant of the resonance between bounded waves and the LM (or Rayleigh wave) is reminiscent of the instability of a piecewise linear shear layer where the resonant interaction of two Rayleigh waves gives an instability of Kelvin–Helmholtz type.

However, note that the description of CLI as an interaction between discrete SG wave modes and an isolated quasi-mode has limited general applicability. Indeed when we consider the profiles with unbounded velocity $U(y)$ as $y \to \infty$ in § 5.3, the growth rate of the radiative modes is modified by the critical layer term. For these profiles we cannot obtain an equivalent of the quasi-mode. Perhaps an equivalent would be a surface wave in the distant fluid with evanescence before the critical point. If so, the RI would be explained with two effects: (i) destabilisation because of radiation at the second turning point, and (ii) the interaction with a surface wave in the far distant flow, which gives the stabilising or destabilising effect of over-reflection at the critical point. Such a description would bring into agreement two independent views of RI, namely as an over-reflection process in papers such as Le Dizès & Billant (2009), or as a wave/mean flow resonance in, for example, Schecter & Montgomery (2004).

Recent works on stratified vortices show similarities with the system we have studied. For the Rankine vortex presented in Billant & Le Dizès (2009), there is also an isolated mode residing on the discontinuity in vorticity. However this case is very different as the critical point is at a greater radius than the discontinuity and the mode does not interact with the branches of bounded SG waves. Moreover there are no unstable modes that are not radiative. In addition smoothing a Rankine vortex leads to stabilisation whereas for our piecewise linear profile smoothing can lead to amplification. Recent work by Yim & Billant (2013) shows that a bending, non-radiative instability can also exist for an isolated vortex in a stratified anticyclonic fluid, and that this instability is due to a critical layer. Finally, it would be interesting to investigate the existence of CLI for other types of flows, in particular for coherent vortices in shallow water, extending the study of Ford (1994) to smooth profiles with critical layers.

Acknowledgements

We are grateful to S. Le Dizès, J. Mak, A. Soward, J. Thuburn, and M. Turner for useful discussions and references, and to anonymous referees for comments and careful reading of the submitted paper. This project has received funding from the European Union Seventh Framework Programme for research, technological development and demonstration under grant agreement number 272722.

Appendix A. Formulae for growth rates

In this appendix we derive the formulae (4.2) and (4.3), and show that (4.2) and (5.17) are equivalent. Recall the definition of M in (2.11): informally introducing time-dependence with fields proportional to $\exp(-\mathrm{i}kct)$, this satisfies

$$2\,\frac{\mathrm{d}M}{\mathrm{d}t} = -\int_0^\infty (vq^* + v^*q)\,\mathrm{d}y - \Big[uv^* + u^*v\Big]_0^\infty \equiv I + B, \tag{A 1}$$

say. The wave momentum M can change by virtue of transport of potential vorticity through the integral term I, or by radiation through the boundary term B. We consider only the former process, taking a mode that is evanescent as $y \to \infty$. We may write the first, integral term I exactly as

$$I = \int_0^\infty \mathrm{i}k^{-1}|v|^2 Q'\,[(U-c^*)^{-1} - (U-c)^{-1}]\,\mathrm{d}y, \tag{A 2}$$

using (2.10). There is a contribution I_d to this integral from any discontinuity in Q that may be present, and a contribution I_c from integrating above or below a pole at $y=y_c$.

For a contribution from integrating around the critical point, it is crucial whether the singular point in the complex y-plane, y_c, lies above or below the real axis. In the former case (upper sign below) we have $\mathrm{Im}\, y_c \simeq U_c' c_i < 0$, and we must integrate above y_c. In the latter case (lower sign), $\mathrm{Im}\, y_c \simeq U_c' c_i > 0$, and we integrate below y_c. We write

$$(U-c^*)^{-1} - (U-c)^{-1} = \frac{-2\mathrm{i}c_i}{(U-c_r)^2 + c_i^2} \simeq \frac{-2\mathrm{i}c_i}{U_c'^2 \tilde{y}^2 + c_i^2}, \tag{A 3}$$

with $\tilde{y} = y - y_r$, where $U(y_r) = c_r$. The latter approximation follows from the assumption that c_i is small, so that the function is sharply peaked in the vicinity of $y = y_r$. As other quantities in the integral vary slowly we simply integrate this expression (evaluating other quantities at $y = y_c$ at leading order) to give

$$I_c = \mp \frac{2\pi |v_c|^2 Q_c'}{kU_c'}. \tag{A 4}$$

Putting this into (2.12) with appropriate attention to signs gives formula (4.2). Another contribution I_d to I in (A 2) is obtained if Q has a step jump at a location y_d, for example for the profile U_1 in (4.1). In this case we have locally $Q' \simeq Q_d\, \delta(y-y_d)$, and (assuming the discontinuity is not too close to the critical point) the integral I includes a contribution

$$I_d = \frac{2Q_d |v_d|^2 c_i}{k(U_d - c_r)^2}. \tag{A 5}$$

If we have both effects we combine (A 4), (A 5) with (2.12) to give the modified formula (4.3) (noting that $U_d = 0$ for our example profiles).

Finally we consider a smooth profile, and link the formula (4.2) derived above for damping connected with the critical point, to the formula (5.17) based on the full WKBJ analysis and matching. We start by evaluating (4.2) in the WKBJ framework. We need M and v_c. First, we have, exactly

$$v = \mathrm{i}F^{-2}k^{-1}(\partial_y g + U'(U-c)^{-1} g), \tag{A 6}$$

$$u = -U'(U-c)^{-1}F^{-2}k^{-2}(\partial_y g + U'(U-c)^{-1} g) - F^{-2} g. \tag{A 7}$$

Substituting these into M (2.11) and retaining only the leading-order terms for the WKBJ approximation yields, with $c \simeq c_r$,

$$M = -F^{-2} \int_0^\infty (U-c_r)|g|^2\, \mathrm{d}y \simeq -\frac{1}{2}|A|^2 F^{-2} \int_0^{y_t} (U-c_r)(-\varDelta_0)^{-1/2}\, \mathrm{d}y, \tag{A 8}$$

using the leading form (3.7), the fact that the solution is exponentially small outside region I (in which $\varDelta \simeq \varDelta_0$) and that the average of the modulus squared of the cosine oscillations in (3.7) is one half. These approximations are good for large k. From this we may note from (3.9) and (2.14) that

$$M \simeq \tfrac{1}{2} F^{-4} |A|^2 k^{-1}\, \partial \varPhi / \partial c. \tag{A 9}$$

This completes our evaluation of M in the WKBJ framework.

Next we need v_c: we substitute g from (5.8) with $G=0$. We take $\kappa=0$ as we evaluate the growth rate by perturbing about the case where there is no critical layer. This gives

$$g \simeq EW_{0,3/2}(z) = E(1+2z^{-1})\mathrm{e}^{-z/2}, \quad z \equiv 2k\tilde{y}. \tag{A 10}$$

Substituting into (A 6) yields

$$v \simeq 2\mathrm{i}F^{-2}E(W'_{0,3/2} + z^{-1}W_{0,3/2}) = -\mathrm{i}F^{-2}E\mathrm{e}^{-z/2}, \tag{A 11}$$

and so calculating at the critical layer with $\tilde{y}=0$, $z=0$ gives $v_c=-\mathrm{i}F^{-2}E$. Now we substitute v_c and M from (A 9) into (4.2) (noting that κ is given in (5.6)) to obtain

$$c_i = \mp \frac{2\pi\kappa}{\partial\Phi/\partial c}\frac{|E|^2}{|A|^2}. \tag{A 12}$$

Finally, in going through the turning point from region I to region II we have $D=(1/2)A\cos\Phi$ and so $|D|=(1/2)|A|$ while in (5.14) we have D in terms of E. Putting these together yields precisely (5.17).

Appendix B. Connection formulae for Whittaker functions

In this appendix we consider connection formulae for Whittaker functions, which are multiple branched. We use formulae (13.14.13) of Olver (2010) for analytic continuation,

$$(-1)^{m+1}W_{\kappa,\mu}(z\mathrm{e}^{2m\mathrm{i}\pi}) = a_m W_{\kappa,\mu}(z) + b_m W_{-\kappa,\mu}(z\mathrm{e}^{\mathrm{i}\pi}), \tag{B 1}$$

where we do not give the general forms of $a_m(\kappa,\mu)$ and $b_m(\kappa,\mu)$ here. We note that for $m=1$,

$$W_{\kappa,\mu}(z\mathrm{e}^{2\mathrm{i}\pi}) = a_1 W_{\kappa,\mu}(z) + b_1 W_{-\kappa,\mu}(z\mathrm{e}^{\mathrm{i}\pi}), \tag{B 2}$$

which is equivalent to

$$W_{\kappa,\mu}(z) = a_1 W_{\kappa,\mu}(z\mathrm{e}^{-2\mathrm{i}\pi}) + b_1 W_{-\kappa,\mu}(z\mathrm{e}^{-\mathrm{i}\pi}), \tag{B 3}$$

$$W_{\kappa,\mu}(z) = c_1 W_{\kappa,\mu}(z\mathrm{e}^{2\mathrm{i}\pi}) + d_1 W_{-\kappa,\mu}(z\mathrm{e}^{\mathrm{i}\pi}), \tag{B 4}$$

with $c_1=1/a_1$ and $d_1=-b_1/a_1$. For our case $\mu=3/2$, Olver (2010) gives

$$a_1 = c_1^* = \mathrm{e}^{2\mathrm{i}\pi\kappa}, \quad b_1 = d_1^* = 2\pi\mathrm{i}\mathrm{e}^{\mathrm{i}\pi\kappa}/[\Gamma(2-\kappa)\Gamma(-1-\kappa)]. \tag{B 5a,b}$$

Consider a solution

$$g_1(z) = W_{\kappa,\mu}(z) \tag{B 6}$$

of the differential equation (5.7). We have the following asymptotic estimate as $z\to\infty$:

$$g_1(z) \sim \mathrm{e}^{-z/2}z^{\kappa} \equiv G_1(z) \quad (-3\pi/2 < \arg z < 3\pi/2) \tag{B 7}$$

by (13.14.21) of Olver (2010). A second solution of the differential equation may be taken in either of the forms

$$g_2^{\pm}(z) = W_{-\kappa,\mu}(z\mathrm{e}^{\pm\mathrm{i}\pi}). \tag{B 8}$$

These second solutions have the asymptotic behaviours

$$g_2^{\pm}(z) \sim e^{z/2} z^{-\kappa} e^{\mp i\pi\kappa} \equiv G_2(z) e^{\mp i\pi\kappa} \quad (-3\pi/2 \mp \pi < \arg z < 3\pi/2 \mp \pi). \tag{B 9}$$

We note the presence of Stokes lines $\arg z = m\pi$ where the exponential terms in the two asymptotic forms G_1 and G_2 are maximally disparate in modulus, and anti-Stokes lines $\arg z = m\pi + \pi/2$ where the two exponentials have purely imaginary arguments.

Now suppose that a boundary condition requires exponential decay in the right half-plane given by RHP $= \{z : -\pi/2 \leqslant \arg z \leqslant \pi/2\}$ as is the case in § 5.2. The exact solution then is $g_1(z)$ in (B 6). Suppose furthermore that we are analysing a mode with $U_c' c_i < 0$. This means that the critical point y_c in the y-plane is pushed below the real axis, and if we are taking our integral along the real y-axis in search of a normal mode, this corresponds to continuing the Whittaker function above the origin in terms of z. This means increasing $\arg z$, into the left half-plane defined by LHP$^+ = \{z : \pi/2 \leqslant \arg z \leqslant 3\pi/2\}$. As we increase the argument of z we encounter Stokes phenomenon (Berry 1989): the subdominant asymptotic term $G_2(z)$ in (B 9) becomes 'switched on' as we cross the Stokes line $\arg z = \pi$ and takes over the solution at the next anti-Stokes line $\arg z = 3\pi/2$. We then have

$$g_1(z) \sim G_1(z) + bG_2(z) \quad (\pi < \arg z < 2\pi), \tag{B 10}$$

where b is a Stokes multiplier. To find b we use the formula (B 3). For z in LHP$^+$ we have also $-3\pi/2 \leqslant \arg z e^{-2i\pi} \leqslant -\pi/2$ and $-\pi/2 \leqslant \arg z e^{-i\pi} \leqslant \pi/2$ so we can use (B 7) for the two terms in (B 3) to give

$$W_{\kappa,\mu}(z) \sim a_1 e^{-z/2} (z e^{-2i\pi})^{\kappa} + b_1 e^{z/2} (z e^{-i\pi})^{-\kappa} = e^{-z/2} z^{\kappa} + b_1 e^{z/2} (z e^{-i\pi})^{-\kappa}. \tag{B 11}$$

As well as the exponentially growing part in LHP$^+$ we gain an exponentially decaying part and the Stokes multiplier is $b = b_1$.

Note that c_i is so small that the z- and y-axes practically coincide provided one traverses the origin in the correct sense and that it is appropriate to use half of the Stokes multiplier for the solution on the Stokes line (Berry 1989). The resulting connection formula is

$$\text{RHP } e^{-z/2} z^{\kappa} \longrightarrow e^{-z/2} z^{\kappa} + \tfrac{1}{2} b\, e^{z/2} (z\, e^{-i\pi})^{-\kappa} \quad (\arg z = \pi). \tag{B 12}$$

A similar argument for integration below a critical point, $U_c' c_i > 0$, using (B 4) yields

$$\text{RHP } e^{-z/2} z^{\kappa} \longrightarrow e^{-z/2} z^{\kappa} + \tfrac{1}{2} d\, e^{z/2} (z e^{i\pi})^{-\kappa} \quad (\arg z = -\pi). \tag{B 13}$$

Here $b = d^* = b_1$ are given in (B 5) for $\mu = 3/2$. To clarify the branch of $z^{\pm\kappa}$ to be taken, we rewrite these so that the power is taken of a positive real quantity,

$$\text{RHP } e^{-z/2} z^{\kappa} \longrightarrow e^{-z/2} (z e^{-i\pi})^{\kappa} e^{i\pi\kappa} + \tfrac{1}{2} b e^{z/2} (z e^{-i\pi})^{-\kappa} \quad (\arg z = \pi), \tag{B 14}$$

$$\text{RHP } e^{-z/2} z^{\kappa} \longrightarrow e^{-z/2} (z e^{i\pi})^{\kappa} e^{-i\pi\kappa} + \tfrac{1}{2} d e^{z/2} (z e^{i\pi})^{-\kappa} \quad (\arg z = -\pi). \tag{B 15}$$

We note that for small κ as in our analysis in § 5.2, the Stokes multipliers $b = b_1$, $d = d_1$ in (B 5) may be taken at leading order as simply $b = d^* = 2i\pi\kappa e^{i\pi\kappa}$. With the imposition of causality or weak viscosity for flows with $U' \leqslant 0$, as in § 4 we always integrate above a critical point, and so the connection formula used is (5.10).

Appendix C. Matching Whittaker and WKBJ solutions

Here we undertake a more careful matching of the WKBJ solution in (3.10) and the Whittaker function approximation in (5.11), and so derive (5.18). First we keep the leading-order effects of Δ_1 by expanding binomially, to write in place of (5.12),

$$I_1 = k\int_{y_t}^{y}\sqrt{\Delta}\,\mathrm{d}y = k\int_{y_t}^{y}\sqrt{\Delta_0}\,\mathrm{d}y + k^{-1}\int_{y_t}^{y}\frac{1}{2}\Delta_1\Delta_0^{-1/2}\,\mathrm{d}y + \cdots . \tag{C 1}$$

Now the first integral on the right-hand side gives $V_{tc} + k\tilde{y} + \cdots$ as before in (5.12). The last integral on the right-hand side becomes, using the form of Δ_1 in (5.4),

$$I_2 = k^{-1}\int_{y_t}^{y}\frac{1}{2}\Delta_1\Delta_0^{-1/2}\,\mathrm{d}y = \int_{y_t}^{y}(-\kappa\tilde{y}^{-1} + k^{-1}\tilde{y}^{-2})\Delta_0^{-1/2}\,\mathrm{d}y \simeq -\kappa\int_{y_t}^{y}\tilde{y}^{-1}\Delta_0^{-1/2}\,\mathrm{d}y, \tag{C 2}$$

neglecting the small contribution from the $\tilde{y}^{-2}$ term to the integral. The remaining integrand has a singularity of the form $\tilde{y}^{-1}$ as y approaches y_c from below (bearing in mind that $\Delta_0 \to 1$). We may subtract this off by writing

$$I_2 \simeq \kappa\int_{y_t}^{y}\tilde{y}^{-1}(1-\Delta_0^{-1/2})\,\mathrm{d}y - \kappa\int_{y_t}^{y}\tilde{y}^{-1}\,\mathrm{d}y. \tag{C 3}$$

Allowing the upper limit to tend to y_c in the first integral and evaluating the second (noting that $\tilde{y}$ is negative in the appropriate range) gives

$$I_2 \simeq \kappa\int_{y_t}^{y_c}\tilde{y}^{-1}(1-\Delta_0^{-1/2})\,\mathrm{d}y - \kappa\log(-\tilde{y}) + \kappa\log(y_c - y_t). \tag{C 4}$$

Assembling these results and redoing the matching process leads to (5.14)–(5.17) again but with V_{tc} replaced by V'_{tc} in (5.18). Note that the corrections in going from V_{tc} to V'_{tc} go to zero as $k^{-1}\log k$ for large k, thus justifying the form of V_{tc} as the leading-order approximation. Nonetheless matching the prefactors gives an improved approximation to c_i.

REFERENCES

BALMFORTH, N. J. 1999 Shear instability in shallow water. *J. Fluid Mech.* **387**, 97–127.

BALMFORTH, N. J., LLEWELLYN SMITH, S. G. & YOUNG, W. R. 2001 Disturbing vortices. *J. Fluid Mech.* **426**, 95–133.

BASSOM, A. P. & GILBERT, A. D. 1999 The spiral wind-up and dissipation of vorticity and a passive scalar in a strained planar vortex. *J. Fluid Mech.* **398**, 245–270.

BENDER, C. M. & ORSZAG, S. A. 1978 *Advanced Mathematical Methods for Scientists and Engineers*. McGraw-Hill.

BERRY, M. V. 1989 Uniform asymptotic smoothing of Stokes's discontinuities. *Proc. R. Soc. Lond.* A **422**, 7–21.

BILLANT, P. & LE DIZÈS, S. 2009 Waves on a columnar vortex in a strongly stratified fluid. *Phys. Fluids* **21**, 106602.

BRETHERTON, F. P. 1966 Critical layer instability in baroclinic flows. *Q. J. R. Meteorol. Soc.* **92**, 325–334.

BRIGGS, R. J., DAUGHERTY, J. D. & LEVY, R. H. 1970 Role of Landau damping in cross-field electron beams and inviscid shear flow. *Phys. Fluids* **13**, 421–432.

BROADBENT, E. G. & MOORE, D. W. 1979 Acoustic destabilization of vortices. *Phil. Trans. R. Soc. Lond.* A **290**, 353–371.

FJØRTOFT, R. 1950 Application of integral theorems in deriving criteria of stability of laminar flow and for the baroclinic circular vortex. *Geophys. Publ.* **17**, 1–52.

FORD, R. 1994 The instability of an axisymmetric vortex with monotonic potential vorticity in rotating shallow water. *J. Fluid Mech.* **280**, 303–334.

GLATZEL, W. 1985 Sonic instabilities in supersonic shear flows. *Mon. Not. R. Astron. Soc.* **281**, 795–821.

HAYASHI, Y.-Y. & YOUNG, W. R. 1987 Stable and unstable shear modes of rotating parallel flows in shallow waters. *J. Fluid Mech.* **184**, 477–504.

VAN HEIJST, G. J. F. 1991 Laboratory experiments on the tripolar vortex in a rotating fluid. *J. Fluid Mech.* **225**, 301–331.

IGA, K. 1999 Critical layer instability as a resonance between a non-singular mode and continuous modes. *Fluid Dyn. Res.* **25**, 63–86.

KNESSL, C. & KELLER, J. B. 1995 Stability of linear shear flows in shallow water. *J. Fluid Mech.* **303**, 203–214.

KUBOKAWA, A. 1985 Instability of a geostrophic front and its energetics. *Geophys. Astrophys. Fluid Dyn.* **33**, 223–257.

LE DIZÈS, S. & BILLANT, P. 2009 Radiative instability in stratified vortices. *Phys. Fluids* **21**, 096602.

LIN, C. C. 1945 On the stability of two-dimensional parallel flows. *Q. Appl. Maths* **3**, 117–142.

LINDZEN, R. S. & BARKER, J. W. 1985 Instability and wave over-reflection in stably stratified shear flow. *J. Fluid Mech.* **151**, 189–217.

LINDZEN, R. S. & TUNG, K. K. 1978 Wave over-reflection and shear instability. *J. Atmos. Sci.* **35**, 1626–1632.

MAK, J., GRIFFITHS, S. D. & HUGHES, D. W. 2014 Shear instabilities in shallow water MHD. *J. Fluid Mech.* (in preparation).

OLVER, F. W. J. 2010 *NIST Handbook of Mathematical Functions*. Cambridge University Press.

PAPALOIZOU, J. C. B. & PRINGLE, J. E. 1987 The dynamical stability of differentially rotating disks III. *Mon. Not. R. Astron. Soc.* **225**, 267–283.

PARK, J. & BILLANT, P. 2012 Radiative instability of an anticyclonic vortex in a stratified rotating fluid. *J. Fluid Mech.* **707**, 381–392.

PARK, J. & BILLANT, P. 2013 The stably stratified Taylor–Couette flow is always unstable except for solid-body rotation. *J. Fluid Mech.* **725**, 262–280.

PARRAS, L. & LE DIZÈS, S. 2010 Temporal instability modes of supersonic round jets. *J. Fluid Mech.* **662**, 173–196.

PERKINS, J. & RENARDY, M. 1997 Stability of equatorial currents with nonzero potential vorticity. *Geophys. Astrophys. Fluid Dyn.* **85**, 31–64.

RAYLEIGH, LORD 1880 On the stability, or instability, of certain fluid motions. *Proc. Lond. Math. Soc.* **11**, 57–70.

RIEDINGER, X., LE DIZÈS, S. & MEUNIER, P. 2010*a* Viscous stability properties of a Lamb–Oseen vortex in a stratified fluid. *J. Fluid Mech.* **645**, 255–278.

RIEDINGER, X., LE DIZÈS, S. & MEUNIER, P. 2011 Radiative instability of the flow around a rotating cylinder in a stratified fluid. *J. Fluid Mech.* **672**, 130–146.

RIEDINGER, X., MEUNIER, P. & LE DIZÈS, S. 2010*b* Instability of a vertical columnar vortex in a stratified fluid. *Exp. Fluids* **49**, 673–681.

ROSSI, L. F., LINGEVITCH, J. F. & BERNOFF, A. J. 1997 Quasi-steady monopole and tripole attractors for relaxing vortices. *Phys. Fluids* **9**, 2329–2338.

SATOMURA, T. 1981 An investigation of shear instability in a shallow water. *J. Meterol. Soc. Japan* **59**, 148–167.

SCHECTER, D. A., DUBIN, D. H. E., CASS, A. C., DRISCOLL, C. F., LANSKY, I. M. & O'NEIL, T. M. 2000 Inviscid damping of asymmetries on a two-dimensional vortex. *Phys. Fluids* **12**, 2397–2412.

SCHECTER, D. A. & MONTGOMERY, M. T. 2004 Damping and pumping of a vortex Rossby wave in a monotonic cyclone: critical layer stirring versus inertial–buoyancy wave emission. *Phys. Fluids* **16**, 1334–1348.

SHEPARD, H. K. 1983 Decay widths for metastable states. Improved WKB approximation. *Phys. Rev.* D **27**, 1288–1298.

SUTHERLAND, B. R. 2010 *Internal Gravity Waves*. Cambridge University Press.

TAKEHIRO, S.-I. & HAYASHI, Y.-Y. 1992 Over-reflection and shear instability in a shallow-water model. *J. Fluid Mech.* **236**, 259–279.

TURNER, M. R., GILBERT, A. D. & BASSOM, A. P. 2008 Neutral modes of a two-dimensional vortex and their link to persistent cat's eyes. *Phys. Fluids* **20**, 027101.

VANNESTE, J. 2013 Balance and spontaneous wave generation in geophysical flows. *Annu. Rev. Fluid Mech.* **45**, 147–172.

YIM, E. & BILLANT, P. 2013 Spontaneous bending of a columnar vortex in stratified-rotating fluid. *Bull. Am. Phys. Soc.* **58** (18), 367.